Lewis Acid Behavior of ReO_2F_3: Synthesis of $(ReO_2F_3)_\infty$, $ReO_2F_4^-$, $Re_2O_4F_7^-$, $Re_3O_6F_{10}^-$, and $ReO_2F_3(CH_3CN)$ and Study by NMR Spectroscopy, Raman Spectroscopy, and Density Functional Theory Calculations; and X-ray Structures of $[Li][ReO_2F_4]$, $[K][Re_2O_4F_7]$, $[K][Re_2O_4F_7]\cdot 2ReO_2F_3$, $[Cs][Re_3O_6F_{10}]$, and $ReO_3F(CH_3CN)_2\cdot CH_3CN$†

William J. Casteel, Jr.,[1] David A. Dixon,[2] Nicolas LeBlond,[1] Philippa E. Lock,[1] Hélène P. A. Mercier,[1] and Gary J. Schrobilgen*,[1]

Department of Chemistry, McMaster University, Hamilton, Ontario L8S 4M1, Canada, and William R. Wiley Environmental Molecular Sciences Laboratory, Pacific Northwest National Laboratory, 906 Batelle Blvd., P.O. Box 999, KI-83, Richland, Washington 99352

Received June 18, 1998

The reaction of Re_2O_7 with XeF_6 in anhydrous HF provides a convenient route to high-purity ReO_2F_3. The fluoride acceptor and Lewis base properties of ReO_2F_3 have been investigated leading to the formation of $[M][ReO_2F_4]$ [M = Li, Na, Cs, $N(CH_3)_4$], $[K][Re_2O_4F_7]$, $[K][Re_2O_4F_7]\cdot 2ReO_2F_3$, $[Cs][Re_3O_6F_{10}]$, and $ReO_2F_3(CH_3CN)$. The $ReO_2F_4^-$, $Re_2O_4F_7^-$, and $Re_3O_6F_{10}^-$ anions and the $ReO_2F_3(CH_3CN)$ adduct have been characterized in the solid state by Raman spectroscopy, and the structures $[Li][ReO_2F_4]$, $[K][Re_2O_4F_7]$, $[K][Re_2O_4F_7]\cdot 2ReO_2F_3$, $[Cs][Re_3O_6F_{10}]$, and $ReO_3F(CH_3CN)_2\cdot CH_3CN$ have been determined by X-ray crystallography. $[Li][ReO_2F_4]$ crystallizes in the tetragonal system, space group $P\bar{4}2_1m$, with $a = 4.727(3)$ Å, $c = 8.880(7)$ Å, $V = 198.4(7)$ Å^3, and $Z = 2$ at 24 °C, $R_1 = 0.0378$, and w$R_2 = 0.1029$. $[K][Re_2O_4F_7]$ crystallizes in the monoclinic system, space group $P2/n$, with $a = 5.4990(11)$ Å, $b = 5.1530(10)$ Å, $c = 14.753(3)$ Å, $\beta = 95.68°$, $V = 415.99(14)$ Å^3, and $Z = 2$ at 20 °C, $R_1 = 0.0473$, and w$R_2 = 0.1200$. $[K][Re_2O_4F_7]\cdot 2ReO_2F_3$ crystallizes in the monoclinic system, space group $C2$, with $a = 27.32(2)$ Å, $b = 5.274(5)$ Å, $c = 5.355(3)$ Å, $\beta = 99.53(4)°$, $V = 760.9(11)$ Å^3, and $Z = 2$ at −60 °C, $R_1 = 0.0238$, and w$R_2 = 0.0645$. $[Cs][Re_3O_6F_{10}]$ crystallizes in the triclinic system, space group $P\bar{1}$, with $a = 7.011(1)$ Å, $b = 9.773(2)$ Å, $c = 10.331(2)$ Å, $\alpha = 113.73(1)°$, $\beta = 91.05(2)°$, $\gamma = 92.42(2)°$, $V = 647.4(2)$ Å^3, and $Z = 2$ at −118 °C, $R_1 = 0.0522$, and w$R_2 = 0.0529$. $ReO_3F(CH_3CN)\cdot CH_3CN$ crystallizes in the orthorhombic system, space group $Pnma$, with $a = 9.138(3)$ Å, $b = 12.518(5)$ Å, $V = 1045.4(7)$ Å^3, and $Z = 4$ at −63 °C, $R_1 = 0.0198$, and w$R_2 = 0.0605$. The structure of $ReO_2F_4^-$ consists of a *cis*-dioxo arrangement of Re−O double bonds in which the Re−F bonds trans to the oxygen atoms are significantly lengthened as a result of the trans influence of the oxygens. The $Re_2O_4F_7^-$ and $Re_3O_6F_{10}^-$ anions and polymeric ReO_2F_3 are open chains containing fluorine-bridged ReO_2F_4 units in which each pair of Re−O bonds are cis to each other and the fluorine bridges are trans to oxygens. The trans influence of the oxygens is manifested by elongated terminal Re−F bonds trans to Re−O bonds as in $ReO_2F_4^-$ and by the occurrence of both fluorine bridges trans to Re−O bonds. Fluorine-19 NMR spectra show that $ReO_2F_4^-$, $Re_2O_4F_7^-$, and $ReO_2F_3(CH_3CN)$ have *cis*-dioxo arrangements in CH_3CN solution. Density functional theory calculations at the local and nonlocal levels confirm that the *cis*-dioxo isomers of $ReO_2F_4^-$ and $ReO_2F_3(CH_3CN)$, where CH_3CN is bonded trans to an oxygen, are the energy-minimized structures. The adduct $ReO_3F(CH_3CN)_2\cdot CH_3CN$ was obtained by hydrolysis of $ReO_2F_3(CH_3CN)$, and was shown by X-ray crystallography to have a facial arrangement of oxygen atoms on rhenium.

Introduction

All of the neutral Re(VII) oxide fluorides, ReO_3F, ReO_2F_3, and $ReOF_5$, have been synthesized and structurally characterized. Selig and El-Gad[3] characterized ReO_3F as the solvolysis product of ReO_4^- in anhydrous HF by Raman spectroscopy and pure solid samples were obtained by the reaction of $KReO_4$ with IF_5 in the presence of trace amounts of HF.[4] Peacock[5] first prepared $ReO_2F_4^-$ by reaction of $[M][ReO_4]$ (M = K, Rb, Cs, Ag) with BrF_3, but the anion was not structurally characterized. A similar synthetic approach involving the reaction of a 1:1 mixture of Re_2O_7 and KBr with an excess of BrF_3 was used by Beattie and co-workers[6] to prepare ReO_2F_3, who characterized the ReO_2F_3 monomer by matrix-isolation Raman and infrared spectroscopy. The vibrational frequencies of the ReO_2F_3 monomer have been subsequently reassigned with the aid of density functional theory (DFT) calculations.[7] To date the most reliable preparations of ReO_2F_3 and $ReOF_5$ have involved direct fluorinations using a 4:1 F_2:Re_2O_7 molar ratio at 200 °C for 65 h for ReO_2F_3 and a 1.1:1 F_2:ReO_2 molar ratio at 250 °C for 12 h for $ReOF_5$.[8] The low volatility and high melting point of

† Dedicated to the memory of Professor Colin J. L. Lock (Oct 4, 1933−May 1, 1996) and his longstanding interests in and contributions to technetium and rhenium chemistry.

(1) McMaster University.
(2) Pacific Northwest Laboratory.
(3) Selig, H.; El-Gad, U. *J. Inorg. Nucl. Chem.* **1973**, *35*, 3517.
(4) Aynsley, E. E.; Hair, M. L. *J. Chem. Soc.* **1958**, 3747.
(5) Peacock, R. D. *J. Chem. Soc.* **1955**, 602.
(6) Beattie, I. R.; Crocombe, R. A.; Ogden, J. S. *J. Chem. Soc., Dalton Trans.* **1977**, 1481.
(7) Casteel, W. J., Jr.; Dixon, D. A.; Mercier, H. P. A.; Schrobilgen, G. J. *Inorg. Chem.* **1996**, *35*, 4310.
(8) Sunder, W. A.; Stevie, F. A. *J. Fluorine Chem.* **1975**, *6*, 449.

10.1021/ic980695t CCC: $18.00
Published on Web 04/17/1999

ReO_2F_3 contrasts with those of ReO_3F and $ReOF_5$ and indicate that ReO_2F_3, like its technetium analogue, TcO_2F_3, is polymeric in the solid state. Although the polymeric structure of TcO_2F_3 has been previously confirmed by its X-ray crystal structure,[9] the detailed structure of polymeric ReO_2F_3 (denoted below as $(ReO_2F_3)_\infty$) has not been determined. The vibrational spectra of the $ReO_2F_4^-$ anion have since been reported,[10] and a ^{19}F NMR study of the $ReO_2F_4^-$ anion, obtained by the reaction of Re_2O_7 with HF in ethanol, has also been reported.[11]

The existing vibrational and solution NMR data indicate that in the Re(VII) oxide fluoride species, where cis- or trans-arrangements of two or three doubly bonded oxygen ligands are possible, the *cis*-dioxo and *fac*-trioxo isomers are favored, for example, the trigonal bipyramidal ReO_2F_3[6] and $ReO_2(OTeF_5)_3$[12] monomers and the pseudooctahedral $ReO_2F_4^-$,[10] $ReO_2(OTeF_5)_4^-$,[12] and $ReO_3F_3^{2-}$ [10] anions. Moreover, the X-ray structures of the polymeric oxofluorometalates $VO_2F_3^{2-}$,[13] $MoOF_4$,[14] $ReOF_4$,[15] $TcOF_4$,[16] WOF_4,[17] $Re_2O_2F_9^+$,[18] $W_2O_2F_9^-$,[19] $Os_2O_4F_7^+$,[7] and TcO_2F_3[9] show that the bridging F ligands in these systems are always trans to the doubly bonded O ligands.

Previous work has shown that high-valent metal oxides and oxide fluorides can be fluorinated in anhydrous HF using noble-gas fluorides. In anhydrous HF, XeF_6 fluorinates TcO_3F to give TcO_2F_3[9] and KrF_2 fluorinates OsO_4 and TcO_2F_3 to give OsO_2F_4[20] and $TcOF_5$,[21] respectively. The present paper describes an improved high-yield synthesis of high-purity ReO_2F_3 using an approach analogous to that used to synthesize TcO_2F_3[9] and the structural characterization of $(ReO_2F_3)_\infty$ by Raman spectroscopy and X-ray crystallography. The Lewis acid behavior of ReO_2F_3 toward fluoride ion and CH_3CN was also investigated leading to the structural characterization of the $ReO_2F_4^-$, $Re_2O_4F_7^-$, and $Re_3O_6F_{10}^-$ anions and the $ReO_2F_3(CH_3CN)$ and $ReO_3F(CH_3CN)_2$ adducts.

Results and Discussion

Synthesis of ReO_2F_3. Previous syntheses of ReO_2F_3 have involved direct fluorination of Re_2O_7 or ReO_2 at elevated temperatures, followed by separation of the products by vacuum sublimation.[8,22,23] The heptoxide has also been fluorinated using BrF_3, but the tendency of the Lewis acid ReO_2F_3 to form adducts with excess BrF_3 made complete removal of this reagent difficult.[6]

An improved, high-yield, high-purity synthesis for ReO_2F_3 has now been achieved by the room-temperature fluorination of Re_2O_7 with XeF_6 in anhydrous HF according to eqs 1−3 and is analogous to the preparation of TcO_2F_3.[9] When ratios of

$$Re_2O_7 + 2HF \xrightarrow{HF} H_2O + 2ReO_3F \quad (1)$$

$$H_2O + XeF_6 \xrightarrow{HF} XeOF_4 + 2HF \quad (2)$$

$$ReO_3F + XeF_6 \xrightarrow{HF} ReO_2F_3 + XeOF_4 \quad (3)$$

$$XeF_6 + ReO_2F_3 \xrightarrow{HF} [XeF_5][ReO_2F_4] \quad (4)$$

$$ReO_3F + XeOF_4 \xrightarrow{HF} ReO_2F_3 + XeO_2F_2 \quad (5)$$

XeF_6:Re_2O_7 exceeding 3:1 were used, the soluble $[XeF_5][ReO_2F_4]$ salt was produced according to eq 4 and no further fluorination of ReO_2F_3 to $ReOF_5$ occurred as was determined by ^{19}F NMR spectroscopy of a sample of XeF_6 and ReO_2F_3 (9:1 molar ratio) in HF (see NMR Spectroscopy) and is analogous in behavior to the XeF_6:Tc_2O_7 system.[24]

The use of a 3:1 molar ratio of XeF_6/Re_2O_7 as the upper limit ensured that only volatile $XeOF_4$ was produced, which was readily pumped off along with HF. The ratio XeF_6:Re_2O_7 = 1.5:1 is the practical lower limit, yielding XeO_2F_2 (eq 5), which has a low volatility and is difficult to pump off. ***Caution:*** *ratios lower than 1.5 would likely result in the formation of shock-sensitive and explosive XeO_3.*[25]

The present synthesis provides ReO_2F_3 in quantitative yield as a stable, white, microcrystalline solid which is essentially insoluble in anhydrous HF and has a melting point (113−116 °C) which is consistent with the observations of Stevie and Sunder,[8] who reported an almost white solid and similar melting point (115 °C). The purity of this material is significantly higher than that reported by Peacock et al.,[22] who described ReO_2F_3 as a pale yellow solid melting at 90 °C. Unlike TcO_2F_3,[24] ReO_2F_3 is stable in Pyrex glass and in CH_3CN solutions at room temperature; however, CH_3CN solutions of ReO_2F_3 produce charring at −40 °C in the presence of $[N(CH_3)_4][F]$, and ReO_2F_3 solutions in CH_2Cl_2 undergo rapid decomposition at room temperature to give blue solutions, typical of Re(VI) species.

The pale yellow $[M][ReO_2F_4]$ (M = Na, K, Rb, Cs, Ag) salts have been previously reported and were formed by combination of ReO_2F_3 and the alkali metal fluorides in the solid state at 120−150 °C[26] or in the reaction between $[M][ReO_4]$ and BrF_3 in BrF_3[5] solvent. Although ReO_2F_3 is insoluble in HF, it rapidly dissolves in the presence of alkali metal fluorides to give pale yellow solutions of $[M][ReO_2F_4]$ (M = Li, Na, K, Cs) salts whose solubilities in anhydrous HF increase with cation size. The K^+ and Cs^+ salts were too soluble for effective crystal growth, but crystals of $[Li][ReO_2F_4]$ were readily grown from saturated HF solutions. The $[Na][ReO_2F_4]$ salt, prepared in a similar manner, gave a pale yellow, microcrystalline powder which was shown by X-ray powder diffraction to be isomorphous with the Li^+ salt. The Lewis acid behavior of ReO_2F_3 in HF contrasts with that of TcO_2F_3 whose conjugate base, $TcO_2F_4^-$, undergoes solvolysis in HF according to eq 6 in all

$$TcO_2F_4^- + nHF \xrightarrow{HF} TcO_2F_3 + (HF)_nF^- \quad (6)$$

but very concentrated fluoro-basic solutions.[24] When the

(9) Mercier, H. P. A.; Schrobilgen, G. J. *Inorg. Chem.* **1993**, *32*, 145.
(10) Kuhlmann, W.; Sawodny, W. *J. Fluorine Chem.* **1977**, *9*, 341.
(11) Bol'shakov, A. M.; Glushkova, M. A.; Buslaev, Y. A. *Dokl. Chem. (Engl. Transl.)* **1983**, *272*, 417; *Dokl. Akad. Nauk SSSR* **1983**, *273*, 1134.
(12) Casteel, W. J.; McLeod, D.; Mercier, H. P. A.; Schrobilgen, G. J. *Inorg. Chem.* **1996**, *35*, 7279.
(13) Ryan, R. R.; Mastin, S. H.; Reisfeld, M. J. *Acta Crystallogr.* **1971**, *B27*, 1270.
(14) Edwards, A. J.; Steventon, B. R. *J. Chem. Soc. A* **1968**, 2507.
(15) Edwards, A. J.; Jones, J. R. *J. Chem. Soc. A* **1968**, 2513.
(16) Edwards, A. J.; Jones, J. R.; Sills, R. J. *J. Chem. Soc. A* **1970**, 2521.
(17) Edwards, A. J.; Jones, J. R. *J. Chem. Soc. A* **1968**, 2074.
(18) Schrobilgen, G. J.; Holloway, J. H.; Russell, D. R. *J. Chem. Soc., Dalton Trans.* **1984**, 1411.
(19) Hoskins, B. F.; Linden, A.; O'Donnell, T. A. *Inorg. Chem.* **1987**, *26*, 2223.
(20) (a) Christe, K. O.; Bougon, R. *J. Chem. Soc., Chem. Commun.* **1992**, 1056. (b) Christe, K. O.; Dixon, D. A.; Mack, H. G.; Oberhammer, H.; Pagelot, A.; Sanders, J. C. P.; Schrobilgen, G. J. *J. Am. Chem. Soc.* **1993**, *115*, 11279.
(21) LeBlond, N.; Schrobilgen, G. J. *Chem. Commun.* **1996**, 2479.
(22) Aynsley, E. E.; Peacock, R. D.; Robinson, P. L. *J. Chem. Soc.* **1950**, 1622.
(23) Cady, G. H.; Hargreaves, G. B. *J. Chem. Soc.* **1961**, 1568.
(24) Casteel, W. J., Jr.; Dixon, D. A.; LeBlond, N.; Mercier, H. P. A.; Schrobilgen, G. J. *Inorg. Chem.* **1998**, *37*, 340.
(25) Smith, D. F. *J. Am. Chem. Soc.* **1963**, *85*, 816.
(26) Yagodin, G. A.; Opalovskii, A. A.; Rakov, É.G.; Dudin, A. S. *Dokl. Akad. Nauk SSSR* **1980**, *252*, 1400.

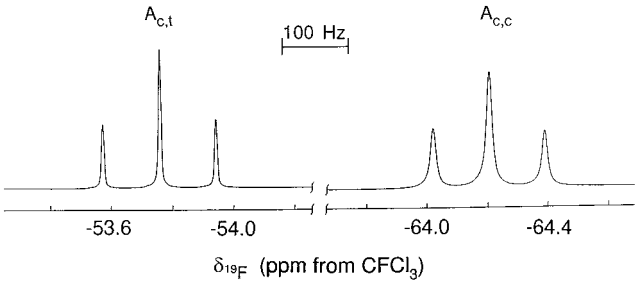

Figure 1. ^{19}F NMR spectrum (470.599 MHz) of $[N(CH_3)_4][ReO_2F_4]$ in CH_3CN solvent recorded at 30 °C, where $A_{c,c}$ and $A_{c,t}$ denote fluorines cis and trans to oxygens, respectively.

ReO_2F_3:F^- molar ratio was increased to 2:1 and to 3:1, the binuclear and trinuclear rhenium anions, $Re_2O_4F_7^-$ and $Re_3O_6F_{10}^-$, were formed according to eqs 7 and 8. A 1.9:1 molar ratio of

$$2ReO_2F_3 + F^- \xrightarrow{HF} Re_2O_4F_7^- \quad (7)$$

$$3ReO_2F_3 + F^- \xrightarrow{HF} Re_3O_6F_{10}^- \quad (8)$$

KF and ReO_2F_3 in HF resulted in the cocrystallization of $[K][Re_2O_4F_7]$ and ReO_2F_3. The nature and concentration of the cation as well as the relative amount of ReO_2F_3 used influences the degree of anion oligomerization in solution. The isolation of $[K][Re_2O_4F_7]\cdot 2ReO_2F_3$ from HF solution when a 4-fold molar excess of ReO_2F_3 with respect to KF is used indicates that the $Re_2O_4F_7^-$ anion is the highest oligomer present in HF solution when KF is used as the fluoro base. In contrast, the $Re_3O_6F_{10}^-$ anion can only be obtained by using the stronger fluoro base CsF. This behavior suggests that significant ion pairing occurs between K^+ and $Re_2O_4F_7^-$, rendering the $Re_2O_4F_7^-$ anion insufficiently fluoro basic to disrupt the ReO_2F_3 polymer and coordinate another ReO_2F_3 unit. Conversely, the weaker Lewis acidity of Cs^+ and accompanying weaker ion-pair interactions result in a fluoride base strength for the $Re_2O_4F_7^-$ anion which is still sufficient to coordinate another ReO_2F_3 unit, forming the $Re_3O_6F_{10}^-$ anion.

The Lewis acid character of ReO_2F_3 is also evident from its solubility in CH_3CN solvent. The complex $ReO_2F_3(CH_3CN)$ was isolated as a white solid by removal of the solvent at 0 °C. Unlike the technetium analogue,[24] $ReO_2F_3(CH_3CN)$ can be stored at room temperature without dissociation to ReO_2F_3 and CH_3CN, consistent with a stronger Re−N bond and the anticipated greater Lewis acidity of ReO_2F_3 compared to that of TcO_2F_3. When the molar ratio of ReO_2F_3 to $[N(CH_3)_4][ReO_2F_4]$ was increased to 2:1 in CH_3CN solution, there was no evidence for the formation of $[N(CH_3)_4][Re_3O_6F_{10}]$. This is attributed to the stronger Lewis base character of CH_3CN relative to $Re_2O_4F_7^-$ so that additional ReO_2F_3 reacts with the solvent to form the $ReO_2F_3(CH_3CN)$ adduct instead.

Characterization of $ReO_2F_4^-$, $Re_2O_4F_7^-$, and $ReO_2F_3(CH_3CN)$ in Solution by ^{19}F NMR Spectroscopy. $[N(CH_3)_4][ReO_2F_4]$, $[Cs][ReO_2F_4]$, and $[XeF_5][ReO_2F_4]$. The ^{19}F NMR spectrum of $[N(CH_3)_4][ReO_2F_4]$ was recorded at 30 °C in CH_3CN. The spectrum displays two triplets [$^2J(^{19}F_{c,t}-^{19}F_{c,c}) = 87$ Hz] at −53.8 and −64.2 ppm (Figure 1) which are assigned to the fluorine environments trans ($F_{c,t}$) and cis ($F_{c,c}$) to the oxygen ligands, respectively, and establish that the cis geometry is adopted by $ReO_2F_4^-$ in solution (structure I). The triplet corresponding to the $F_{c,c}$ environment is broadened ($\Delta\nu_{1/2}$, 10.7 Hz) compared with that of $F_{c,t}$ ($\Delta\nu_{1/2}$, 5.8 Hz). The broadening is attributed to residual scalar coupling of ^{19}F to the quadrupolar nuclei ^{185}Re (37.4%, $I = {}^5/_2$, $Q = 2.8 \times 10^{-28}$ m^2) and ^{187}Re (62.6%, $I = {}^5/_2$, $Q = 2.6 \times 10^{-28}$ m^2).[27] It is anticipated that $^1J(^{185,187}Re-^{19}F_{c,t}) < {}^1J(^{185,187}Re-^{19}F_{c,c})$ because the Re−$F_{c,c}$ bonds are expected to be more covalent than the Re−$F_{c,t}$ bonds, which are trans to oxygen. The greater length of the Re−$F_{c,t}$ bonds relative to those of Re−$F_{c,c}$ was confirmed in the X-ray crystal structure of $[Li][ReO_2F_4]$ (see X-ray Crystal Structures). The correspondingly smaller $^1J(^{19}F_{c,t}-^{185,187}Re)$ coupling constants are also expected by analogy with the trend observed in the ^{19}F NMR spectrum of $TcO_2F_4^-$,[24] which consists of a partly quadrupole-collapsed $^1J(^{99}Tc-^{19}F_{c,c})$ coupling on the *cis*-fluorine resonance and a significantly smaller $^1J(^{99}Tc-^{19}F_{c,t})$ coupling on the *trans*-fluorine resonance that is almost completely quadrupole collapsed. The smaller $^1J(M-^{19}F_{c,t})$ couplings are affected to the same extent by quadrupolar relaxation of the M atoms as the larger $^1J(M-^{19}F_{c,c})$ couplings, resulting in a narrower line width for the $F_{c,t}$ resonances in both $TcO_2F_4^-$ and $ReO_2F_4^-$.

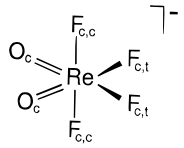

Structure I

The ^{19}F NMR spectrum of a 1:5 molar ratio of ReO_2F_3 and CsF in HF at 30 °C consists of a singlet at −35.6 ppm ($\Delta\nu_{1/2}$, 10 Hz) assigned to the $F_{c,c}$ environment of $ReO_2F_4^-$. Only one other resonance was observed at −195.1 ppm ($\Delta\nu_{1/2}$, 60 Hz) and was assigned to the $F_{c,t}$ environment of $ReO_2F_4^-$ undergoing rapid fluorine exchange with the solvent. This exchange is slowed sufficiently at −80 °C to observe two triplets at −30.7 ppm ($\Delta\nu_{1/2}$, 65 Hz) and −135.7 ($\Delta\nu_{1/2}$, 50 Hz), assigned to the *cis*- and *trans*-fluorines, respectively, and the HF solvent resonance at −190.9 ppm ($\Delta\nu_{1/2}$, 30 Hz). The exchange behavior parallels that of $[Cs][TcO_2F_4]$ in HF in the presence of excess CsF[24] and confirms the assignment of the more labile fluorine environment to the fluorines trans to oxygen. As in the case of $TcO_2F_4^-$, the $F_{c,t}$ environment occurs at lower frequency than that of $F_{c,c}$. The coupling constant, $^2J(^{19}F_c-^{19}F_t) = 85$ Hz, is in excellent agreement with that observed for $[N(CH_3)_4][ReO_2F_4]$ in CH_3CN. The ^{19}F NMR spectrum of a 1:9 molar ratio of ReO_2F_3 and XeF_6 in HF at 30 °C consists of a singlet at −31.9 ppm ($\Delta\nu_{1/2}$, 12 Hz) assigned to $F_{c,c}$ of $ReO_2F_4^-$. Only one other resonance was observed at −120.8 ppm ($\Delta\nu_{1/2}$, 210 Hz) and is assigned to the *trans*-fluorines of $ReO_2F_4^-$ undergoing rapid fluorine exchange with XeF_6, XeF_5^+, and HF. Although the $^2J(^{19}F_{c,t}-^{19}F_{c,c})$ coupling constant values obtained in HF and CH_3CN solvents are in very good agreement with the value reported by Buslaev et al.[11] (89 Hz) for a solution of Re_2O_7 in 60% HF in ethanol (−32.2 ppm, triplet; −109.2 ppm, triplet), the ^{19}F chemical shifts are noted to be highly solvent dependent.

$ReO_2F_3(CH_3CN)$. There are three isomers possible for $ReO_2F_3(CH_3CN)$ which would produce the same multiplicities and relative intensities in the ^{19}F NMR spectrum, a *trans*-dioxo isomer and two *cis*-dioxo isomers in which CH_3CN is coordinated trans to an oxygen or trans to a fluorine. The energy-minimized structure arrived at by LDFT calculations for gas-phase $ReO_2F_3(CH_3CN)$ is a *cis*-dioxo isomer in which CH_3CN is coordinated trans to an oxygen and is the assumed structure (see structure II and Computational Results) and is analogous to the energy-minimized structure predicted for $TcO_2F_3(CH_3CN)$.[24] Moreover, no examples of pseudooctahedral *trans*-dioxo d^0 species are known.

(27) Rehder, D. In *Multinuclear NMR*; Mason, J., Ed.; Plenum: New York, 1987; p 512.

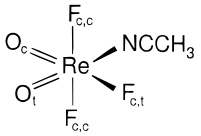

Structure II

The ^{19}F NMR spectrum of $ReO_2F_3(CH_3CN)$ was recorded in SO_2ClF solvent in the presence of excess CH_3CN at 30 °C (and at −80 °C; values in brackets). The spectrum consists of an AB_2 pattern at 282.409 MHz with the $F_{c,c}$ environment at −23.8 ($\Delta\nu_{1/2}$, 18 Hz) [−24.1 ($\Delta\nu_{1/2}$, 13 Hz)] ppm (doublet) and the $F_{c,t}$ environment at −25.8 ($\Delta\nu_{1/2}$, 27 Hz) [−34.3 ($\Delta\nu_{1/2}$, 15 Hz)] ppm (triplet) with relative integrated intensities of 2.0:1.0 (structure II) and a two-bond $^2J(^{19}F_{c,t}-^{19}F_{c,c})$ coupling constant of 119 [117] Hz. A similar dependence of the $F_{c,t}$ resonance has been observed for $TcO_2F_3(CH_3CN)$.[24] The ^{19}F NMR spectrum of $ReO_2F_3(CH_3CN)$ was also recorded in CH_3CN solvent at 30 °C, yielding an AX_2 pattern at 282.409 MHz with NMR parameters (−24.5 (doublet) and −31.1 (triplet) ppm, $^2J(^{19}F_{c,t}-^{19}F_{c,c}) = 115$ Hz) very similar to those obtained for the adduct in SO_2ClF solvent. The ^1H NMR spectrum of $ReO_2F_3(CH_3CN)$ recorded in SO_2ClF in the presence of excess CH_3CN shows two singlets at 2.40 and 1.81 ppm assigned to complexed and free CH_3CN, respectively. The proton-decoupled ^{13}C NMR spectrum of this solution shows the complexed acetonitrile signals at 1.81 (CH_3) and 119.0 (CN) ppm and free CH_3CN at 0.46 (CH_3) and 117.5 (CN) ppm. The ^1H and ^{13}C complexation shifts for $ReO_2F_3(CH_3CN)$ with respect to free CH_3CN are consistent with Lewis acid−base adduct formation. Moreover, the narrow line widths of the ^1H ($\Delta\nu_{1/2}$, 5 Hz) and ^{13}C ($\Delta\nu_{1/2}$, 11 Hz) resonances indicate that the rate of exchange between free and complexed CH_3CN is slow on the NMR time scale.

$[N(CH_3)_4][Re_2O_4F_7]$. The ^{19}F NMR spectrum of a 1:1 molar ratio of ReO_2F_3 and $[N(CH_3)_4][ReO_2F_4]$ recorded in CH_3CN solvent at −40 °C is an equilibrium mixture of three species: $ReO_2F_3(CH_3CN)$ [65 mol %; $F_{c,c}$ doublet, −24.3 ppm ($\Delta\nu_{1/2}$, 15 Hz); $F_{c,t}$ triplet −34.7 ppm ($\Delta\nu_{1/2}$, 15 Hz); $^2J(^{19}F_{c,t}-^{19}F_{c,c})$, 118 Hz], $ReO_2F_4^-$ [12 mol %; $F_{c,c}$ triplet, −66.3 ppm ($\Delta\nu_{1/2}$, 5 Hz); $F_{c,t}$ triplet −52.1 ppm ($\Delta\nu_{1/2}$, 5 Hz); $^2J(^{19}F_c-^{19}F_t)$, 87 Hz], and $Re_2O_4F_7^-$ (23 mol %) (Figure 2). The ^{19}F NMR spectrum of the $Re_2O_4F_7^-$ anion (structure III) comprises a doublet of

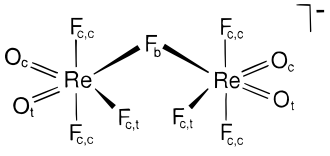

Structure III

doublets at −28.8 ppm ($\Delta\nu_{1/2}$, 9 Hz) assigned to the terminal fluorines cis to the oxygens ($F_{c,c}$), a doublet of triplets at −38.6 ppm ($\Delta\nu_{1/2}$, 12 Hz) assigned to the terminal fluorines trans to O_c ($F_{c,t}$), and a triplet of quintets at −141.2 ppm ($\Delta\nu_{1/2}$, 12 Hz) assigned to the bridging fluorine (F_b). The high shielding of the F_b resonance is characteristic of fluorine-bridged species (e.g., $Mo_2O_2F_9^-$ [28] and $W_2O_2F_9^-$ [29]) and is consistent with its more ionic bonding. The coupling constants $^2J(^{19}F_{c,t}-^{19}F_{c,c})$ and

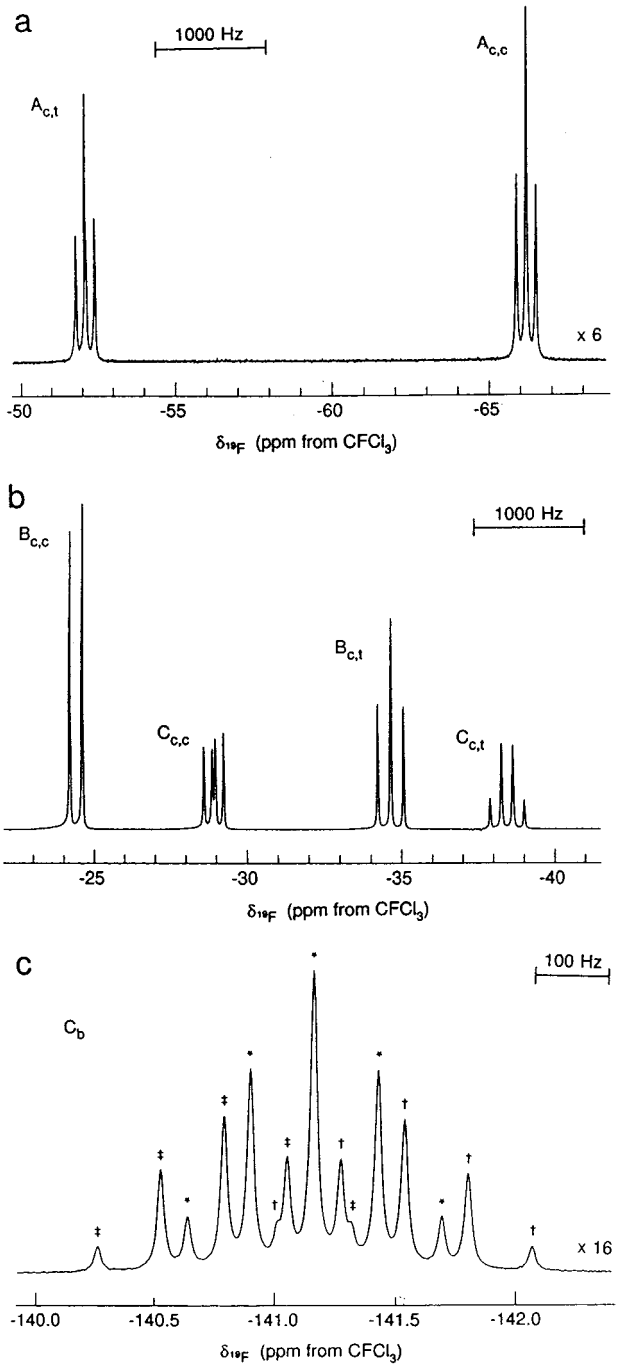

Figure 2. ^{19}F NMR spectrum (282.409 MHz) of $[N(CH_3)_4][Re_2O_4F_7]$ in CH_3CN solvent recorded at −40 °C: (a) fluorines cis ($A_{c,c}$) and trans ($A_{c,t}$) to oxygens in $ReO_2F_4^-$; (b) fluorines cis ($B_{c,c}$) and trans ($B_{c,t}$) to oxygens in $ReO_2F_3(CH_3CN)$ and fluorines cis ($C_{c,c}$) and trans ($C_{c,t}$) to oxygens in $Re_2O_4F_7^-$; (c) fluorine bridge (C_b) in $Re_2O_4F_7^-$, where ∗, †, and ‡ denote the individual quintet patterns of the triplet of quintets associated with this resonance.

$^2J(^{19}F_{c,t}-^{19}F_b)$ are identical within experimental error (105 Hz), while $^2J(^{19}F_{c,c}-^{19}F_b)$ is significantly smaller (75 Hz).

X-ray Crystal Structures. Details of the data collection parameters and other crystallographic information for [Li]-$[ReO_2F_4]$, [K]$[Re_2O_4F_7]$, [K]$[Re_2O_4F_7]\cdot 2ReO_2F_3$, [Cs]$[Re_3O_6F_{10}]$, and $ReO_3F(CH_3CN)_2\cdot CH_3CN$ are given in Table 1. Important bond lengths, angles, significant long contacts, and bond valences, as defined by Brown,[33] for individual bonds and anion−cation contacts are given in Table 2.

(28) Buslaev, Yu. A.; Kokunov, Yu. V.; Bochkareva, V. A. *J. Struct. Chem.* **1972**, *13*, 570; *Zh. Strukt. Khim.* **1972**, *13*, 611.
(29) Buslaev, Yu. A.; Kokunov, Yu. V.; Bochkareva, V. A.; Shostorovich, E. M. *J. Struct. Chem.* **1972**, *13*, 491; *Zh. Strukt. Khim.* **1972**, *13*, 526.
(30) Holloway, J. H.; Schrobilgen, G. J. *Inorg. Chem.* **1980**, *19*, 2632.
(31) Holloway, J. H.; Schrobilgen, G. J. *Inorg. Chem.* **1981**, *20*, 3363.

Table 1. Summary of Crystal Data and Refinement Results for $[Li][ReO_2F_4]$, $[K][Re_2O_4F_7]$, $[K][Re_2O_4F_7]\cdot 2ReO_2F_3$, $[Cs][Re_3O_6F_{10}]$, and $ReO_3F(CH_3CN)_2\cdot CH_3CN$

	$[Li][ReO_2F_4]$	$[K][Re_2O_4F_7]$	$[K][Re_2O_4F_7]\cdot 2ReO_2F_3$	$[Cs][Re_3O_6F_{10}]$	$ReO_3F(CH_3CN)_2\cdot CH_3CN$
space group	$P\bar{4}2_1m$	$P2/n$	$C2$	$P\bar{1}$	$Pnma$
a (Å)	4.727(3)	5.4990(11)	27.32(2)	7.011(1)	9.138(3)
b (Å)	4.727(3)	5.1530(10)	5.274(5)	9.773(2)	12.518(5)
c (Å)	8.880(7)	14.753(3)	5.355(3)	10.331(2)	9.138(4)
α (deg)	90.0	90.0	90.0	113.73(1)	90.0
β (deg)	90.0	95.68(3)	99.53(4)	91.05(2)	90.0
γ (deg)	90.0	90.0	90.0	92.42(2)	90.0
V (Å^3)	198.4(7)	415.99(14)	760.9(11)	647.4(2)	1045.4(7)
molecules/unit cell	2	2	2	2	4
molecular wt (g mol^{-1})	301.14	608.50	1158.90	977.51	373.34
ρ_{calcd} (g cm^{-3})	5.040	4.858	5.058	5.018	2.372
T (°C)	24	20	−60	−118	−63
μ (cm^{-1})	1.648	1.5961	3.217	1.661	1.1625
λ (Å)	0.560 86	0.560 86	0.710 73	0.560 86	0.710 73
final agreement factors[a]	$R_1 = 0.0378$	$R_1 = 0.0473$	$R_1 = 0.0238$	$R_1 = 0.0522$	$R_1 = 0.0198$
	$wR_2 = 0.1029$	$wR_2 = 0.1200$	$wR_2 = 0.0645$	$wR_2 = 0.0529$	$wR_2 = 0.0605$

[a] $R_1 = \sum||F_o| - |F_c||/\sum|F_o|$ for $I > 2\sigma(I)$. $wR_2 = [\sum[w(F_o^2 - F_c^2)^2]/\sum w(F_o^2)^2]^{1/2}$ for $I > 2\sigma(I)$.

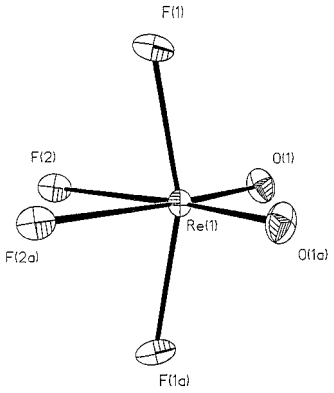

Figure 3. Geometry of the $ReO_2F_4^-$ anion in $[Li][ReO_2F_4]$. Thermal ellipsoids are shown at the 50% probability level.

$[Li][ReO_2F_4]$, $[K][Re_2O_4F_7]$, $[K][Re_2O_4F_7]\cdot 2ReO_2F_3$, and $[Cs][Re_3O_6F_{10}]$. (a) Crystal Packing. The bilayer packing arrangement of $[Li][ReO_2F_4]$ (Figure 3) is identical to that of $[Li][TcO_2F_4]$[24] with a minimum O···O distance of 3.065 Å (cf. the sum of the van der Waals radii for two oxygen atoms: 2.80, 2.84 Å).[34]

The crystal structure of $[K][Re_2O_4F_7]$ consists of layers of $[K][Re_2O_4F_7]$ stacked along the c-axis. The shortest interatomic distance between the layers is between O(2) and O(1) (2.998 Å) and is at the limit of the sum of the van der Waals radii. The $Re_2O_4F_7^-$ anions are connected to each other within the ab-plane through contacts with K^+ cations (Figure S1). There are also several weak contacts between the $Re_2O_4F_7^-$ anions within the same layer (F(2)···F(5), 2.904 Å, and O(2)···F(4), 3.023 Å). The crystal structure is similar to that of $[K][Re_2O_4F_7]\cdot 2ReO_2F_3$ (Figure 4a) which consists of layers of $[K][Re_2O_4F_7]$ and $(ReO_2F_3)_\infty$ which alternate along the a-axis. The shortest interatomic distance between the two layers is between O(1) and F(7) (2.897 Å) and is also at the limit of the sum of the fluorine and oxygen van der Waals radii (2.75, 2.82 Å).[34] Consequently, each component of the structure is considered distinct and will be discussed separately. In this structure, the $Re_2O_4F_7^-$ anions are connected to each other within the bc-plane through contacts with K^+ cations (Figure S2). Weak contacts between the $Re_2O_4F_7^-$ anions also occur within the same plane (O(2)···F(4), 2.910 Å, and O(2)···F(3), 3.008 Å). The geometrical parameters for $[K][Re_2O_4F_7]$ are identical in both structures and the Re−O and Re−F bond length distortions are reproducible, confirming that they are related to cation−anion interactions or packing effects and do not result from positional disorder between F and O (see Experimental Section).

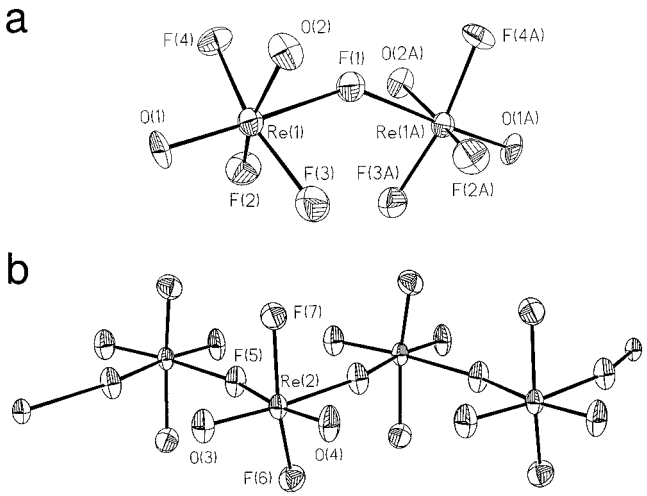

Figure 4. Crystal structure of $[K][Re_2O_4F_7]\cdot 2ReO_2F_3$ showing thermal ellipsoids at the 50% probability level with views of (a) the $Re_2O_4F_7^-$ anion and (b) the polymeric ReO_2F_3 chain.

The $Re_3O_6F_{10}^-$ anions (Figure 5) are packed along the a-axis, and the shortest secondary contacts occur between O(1)···O(4), 2.768 Å, and O(3)···F(3), 2.873 Å.

(b) Anion and Molecular Geometries and Secondary Contacts. The alkali metal cations (M^+) exhibit M···F contacts[35] with the anions in the crystal structures of $[Li][ReO_2F_4]$, $[K][Re_2O_4F_7]$, $[K][Re_2O_4F_7]\cdot 2ReO_2F_3$, and $[Cs][Re_3O_6F_{10}]$. The lithium cation in $[Li][ReO_2F_4]$ has six Li···F contacts with the fluorine atoms forming a slightly distorted octahedron. Although the total bond valence around Li^+ arising from these fluorine

(32) Bacon, J.; Dean, P. A. W.; Gillespie, R. J. *Can. J. Chem.* **1970**, *48*, 3413.

(33) (a) Brown, I. D. *J. Solid State Chem.* **1974**, *11*, 214. (b) Brown, I. D. In *Structure and Bonding in Crystals*; O'Keefe, M., Navrotsky, A., Eds; Academic: London, 1981; Vol. 2, p 1. (c) Brown, I. D.; Altermatt, D. *Acta Crystallogr.* **1985**, *B41*, 244.

(34) (a) Pauling, L. *The Nature of the Chemical Bond*, 3rd ed.; Cornell University Press: Ithaca, NY, 1960; p 260. (b) Bondi, A. *J. Phys. Chem.* **1964**, *68*, 441.

(35) The anion···cation contacts are defined as distances which are smaller or equal to the sum of the ionic radii of the cation ($Li^+ = 1.38$ Å, $K^+ = 1.51$ Å, and $Cs^+ = 1.67$ Å for a coordination number of 6, 8, and 6, respectively) and the van der Waals radius of the F (1.35 or 1.40 Å) or O (1.5 Å) atoms the cation makes contact with.

Table 2. Experimental Bond Lengths (Å), Bond Valences (vu),[a] Long Contacts (Å), and Bond Angles (deg) for $[Li][ReO_2F_4]$, $[K][Re_2O_4F_7]$, $[K][Re_2O_4F_7]\cdot 2ReO_2F_3$, $[Cs][Re_3O_6F_{10}]$, and $ReO_3F(CH_3CN)_2\cdot CH_3CN$ and Calculated Geometries for $ReO_2F_4^-$, $Re_2O_4F_7^-$, and Monomeric ReO_2F_3, $Re_3O_6F_{10}^-$, and $ReO_2F_3(CH_3CN)$[b]

$[Li][ReO_2F_4]$

Bond Lengths (Å), Long Contacts (Å), and Corresponding Bond Valences (vu)[a]

	Re(1)−F(1)	Re(1)−F(2)	Re(1)−O(1)	Li−F(2,2A)	Li−F(1B,1C)	Li−F(2B,2C)
bond valence	0.920	0.638	1.976	0.160	0.157	0.132
bond length	1.867(8)	2.002(7)	1.678(9)	2.04(3)	2.05(2)	2.108(7)
tot. bond valence	Re(1): 7.07			Li: 0.90		

Bond Lengths (Å) and Angles (deg)

		DZVP2				DZVP2	
	expt	LDFT	NLDFT		expt	LDFT	NLDFT
Re(1)−F(1)	1.867(8)	1.913	1.936	F(1)−Re(1)−F(2)	82.8(3)	86.9	85.2
Re(1)−F(2)	2.002(7)	1.965	1.996	F(1)−Re(1)−O(1)	95.5(2)	92.6	93.8
Re(1)−O(1)	1.678(9)	1.737	1.740	F(2)−Re(1)−O(1)	91.7(4)	88.5	89.4
F(1)−Re(1)−F(1A)	162.9(6)	171.8	167.7	F(2)−Re(1)−F(2A)	76.3(4)	82.4	78.5
O(1)−Re(1)−F(2A)	168.1(4)	170.9	168.0	F(1)−Re(1)−O(1A)	96.1(3)	92.6	93.8
O(1)−Re(1)−O(1A)	100.2(7)	100.6	102.6				

$[K][Re_2O_4F_7]$[b]

Bond Lengths (Å), Long Contacts (Å), and Corresponding Bond Valences (vu)[a]

	Re(1)−F(1)	Re(1)−F(2)	Re(1)−F(3)	Re(1)−F(4)	Re(1)−O(1)	Re(1)−O(2)
bond valence	0.422 (0.428)	0.857 (0.881)	1.148 (1.154)	0.922 (0.888)	2.058 (1.987)	1.613 (1.558)
bond length	2.155(4) (2.150(4))	1.893(8) (1.883(7))	1.785(9) (1.783(8))	1.866(8) (1.880(6))	1.663(12) (1.676(7))	1.753(9) (1.766(7))
tot. bond valence	7.02 (6.90)					

	K(1)−F(2B,2C)	K(1)−F(3B,3C)	K(1)−F(4,4A)	K(1)−O(2B,2C)
bond valence	0.129 (0.138)	0.088 (0.107)	0.125 (0.145)	0.104 (0.117)
bond length	2.75(1) (2.724(8))	2.89(1) (2.820(8))	2.76(1) (2.706(7))	2.97(1) (2.925(8))
tot. bond valence	0.89 (1.01)			

Bond Lengths (Å) and Angles (deg)

	expt	LDFT/DZVP		expt	LDFT/DZVP
Re(1)−F(1)	2.155(4) (2.150(4))	2.125	O(1)−Re(1)−O(2)	100.5(5) (99.8(4))	101.9
Re(1)−F(2)	1.893(8) (1.883(7))	1.935	O(2)−Re(1)−F(4)	89.9(4) (89.1(3))	92.1
Re(1)−F(3)	1.785(9) (1.783(8))	1.885	O(1)−Re(1)−F(1)	176.2(3) (176.0(4))	173.2
Re(1)−F(4)	1.866(8) (1.880(6))	1.892	F(1)−Re(1)−F(2)	78.2(4) (78.2(3))	78.1
Re(1)−O(1)	1.663(12) (1.676(7))	1.715	O(1)−Re(1)−F(2)	98.7(5) (99.8(4))	95.6
Re(1)−O(2)	1.766(7) (1.753(9))	1.724	F(1)−Re(1)−F(3)	82.2(4) (83.6(4))	80.6
O(1)−Re(1)−F(3)	99.9(5) (99.8(5))	96.4	F(1)−Re(1)−F(4)	79.1(4) (78.8(3))	84.1
O(1)−Re(1)−F(4)	98.4(5) (97.6(4))	97.7	F(2)−Re(1)−F(3)	86.7(4) (87.5(4))	85.5
O(2)−Re(1)−F(1)	82.4(4) (81.8(3))	84.5	F(2)−Re(1)−F(4)	82.3(4) (81.9(4))	81.8
O(2)−Re(1)−F(2)	160.2(5) (159.4(4))	162.1	F(3)−Re(1)−F(4)	159.9(5) (160.9(4))	161.9
O(2)−Re(1)−F(3)	95.0(4) (95.6(4))	96.0	Re(1)−F(1)−Re(1A)	139.5(6) (143.3(6))	179.8

Polymeric ReO_2F_3 (Expt)[c] and Monomeric ReO_2F_3 (Calcd)[d]

Bond Lengths (Å) and Corresponding Bond Valences (vu)[a]

	Re(2)−F(5)	Re(2)−F(5A)	Re(2)−F(6)	Re(2)−F(7)	Re(2)−O(3)	Re(2)−O(4)
bond valence	0.510	0.467	1.014	0.953	2.036	1.992
bond length	2.085(6)	2.118(7)	1.831(6)	1.854(6)	1.667(8)	1.675(8)
tot. bond valence	6.97					

Bond Lengths (Å) and Angles (deg)

	expt[c]	LDFT/DZVP[d]		expt[c]	LDFT/DZVP[d]
Re(2)−F(5)	2.085(6)	1.894	O(4)−Re(2)−F(6)	98.8(4)	96.0
Re(2)−F(6)	1.831(6)	1.876	O(4)−Re(2)−F(7)	97.8(4)	
Re(2)−F(7)	1.854(6)		O(3)−Re(2)−F(6)	98.1(4)	
Re(2)−O(3)	1.667(8)	1.705	O(3)−Re(2)−F(7)	98.7(4)	
Re(2)−O(4)	1.675(8)		F(5)−Re(2)−F(5A)	79.8(1)	
O(3)−Re(2)−O(4)	102.3(4)	110.5	F(6)−Re(2)−F(7)	153.2(3)	158.8
O(3)−Re(2)−F(5)	88.5(4)	124.7	F(5)−Re(2)−F(6)	80.2(3)	79.4
O(4)−Re(2)−F(5A)	89.4(4)		F(5)−Re(2)−F(7)	79.5(3)	
O(3)−Re(2)−F(5A)	168.2(4)		F(5A)−Re(2)−F(6)	79.8(3)	
O(4)−Re(2)−F(5)	169.1(4)		F(5A)−Re(2)−F(7)	79.5(3)	

Table 2 (Continued)

$[Cs][Re_3O_6F_{10}]$

Bond Lengths (Å), Long Contacts (Å), and Corresponding Bond Valences (vu)[a]

	Re(1)−F(1)	Re(1)−F(2)	Re(1)−F(3)	Re(1)−F(4)	Re(1)−O(1)	Re(1)−O(2)
bond valence	0.927	0.823	0.984	0.361	2.025	1.788
bond length	1.864(7)	1.908(6)	1.842(6)	2.213(6)	1.669(8)	1.715(8)
tot. bond valence	6.91					
	Re(2)−F(4)	Re(2)−F(5)	Re(2)−F(6)	Re(2)−F(7)	Re(2)−O(3)	Re(2)−O(4)
bond valence	0.540	0.960	0.968	0.578	1.892	1.949
bond length	2.064(7)	1.851(7)	1.848(6)	2.039(6)	1.694(8)	1.683(7)
tot. bond valence	6.89					
	Re(3)−F(7)	Re(3)−F(8)	Re(3)−F(9)	Re(3)−F(10)	Re(3)−O(5)	Re(3)−O(6)
bond valence	0.427	0.763	0.960	0.920	1.976	1.887
bond length	2.151(6)	1.936(7)	1.851(7)	1.867(7)	1.678(7)	1.695(9)
tot. bond valence	6.93					
	Cs(1)−F(1A)	Cs(1)−F(5A)	Cs(1)−F(8A)	Cs(1)−F(9A)	Cs(1)−F(10)	Cs(1)−F(8)
bond valence	0.152	0.125	0.158	0.155	0.119	0.118
bond length	3.027(7)	3.099(7)	3.013(7)	3.020(7)	3.117(8)	3.122(7)
tot. bond valence	0.94					

Bond Lengths (Å) and Angles (deg)

	expt	LDFT/DZVP		expt	LDFT/DZVP
Re(1)−F(1)	1.864(7)	1.886	O(1)−Re(1)−O(2)	102.6(4)	101.4
Re(1)−F(2)	1.908(6)	1.922	O(1)−Re(1)−F(1)	98.5(4)	98.4
Re(1)−F(3)	1.842(6)	1.868	O(2)−Re(1)−F(1)	93.1(4)	91.4
Re(1)−F(4)	2.213(6)	2.166	O(1)−Re(1)−F(2)	99.0(4)	99.4
Re(1)−O(1)	1.669(8)	1.711	O(2)−Re(1)−F(2)	158.4(5)	159.1
Re(1)−O(2)	1.715(8)	1.728	F(1)−Re(1)−F(2)	82.0(4)	84.4
O(1)−Re(1)−F(3)	97.9(4)	98.3	O(2)−Re(1)−F(3)	95.6(4)	92.7
F(1)−Re(1)−F(3)	159.2(4)	161.7	F(2)−Re(1)−F(3)	83.0(4)	85.5
O(1)−Re(1)−F(4)	175.4(3)	176.9	O(2)−Re(1)−F(4)	81.9(3)	81.6
F(1)−Re(1)−F(4)	81.6(3)	82.1	F(2)−Re(1)−F(4)	76.5(3)	77.6
F(3)−Re(1)−F(4)	81.0(3)	80.8	Re(1)−F(4)−Re(2)	140.6(3)	177.1
Re(2)−F(4)	2.064(7)	2.064	F(4)−Re(2)−O(3)	89.7(4)	90.8
Re(2)−F(5)	1.851(7)	1.865	F(4)−Re(2)−O(4)	166.9(3)	167.2
Re(2)−F(6)	1.848(6)	1.873	O(3)−Re(2)−O(4)	103.3(4)	101.8
Re(2)−F(7)	2.039(6)	2.080	F(4)−Re(2)−F(5)	80.9(3)	81.2
Re(2)−O(3)	1.694(8)	1.705	O(3)−Re(2)−F(5)	97.5(4)	98.5
Re(2)−O(4)	1.683(7)	1.711	O(4)−Re(2)−F(5)	98.7(4)	94.4
F(4)−Re(2)−F(6)	79.7(3)	84.4	O(3)−Re(2)−F(6)	96.9(4)	94.5
O(4)−Re(2)−F(6)	96.9(4)	97.0	F(5)−Re(2)−F(6)	155.7(3)	160.6
F(4)−Re(2)−F(7)	77.3(3)	79.8	O(3)−Re(2)−F(7)	167.0(4)	169.4
O(4)−Re(2)−F(7)	89.7(4)	87.8	F(5)−Re(2)−F(7)	81.0(3)	85.1
F(6)−Re(2)−F(7)	80.5(4)	79.8	Re(2)−F(7)−Re(3)	178.5(5)	169.3
Re(3)−F(7)	2.151(6)	2.163	F(7)−Re(3)−O(5)	170.8(5)	175.0
Re(3)−F(8)	1.936(7)	1.918	F(7)−Re(3)−O(6)	85.0(4)	82.0
Re(3)−F(9)	1.851(7)	1.880	O(5)−Re(3)−O(6)	104.3(5)	103.0
Re(3)−F(10)	1.867(7)	1.887	F(7)−Re(3)−F(8)	75.9(3)	77.3
Re(3)−O(5)	1.678(7)	1.710	O(5)−Re(3)−F(8)	94.9(4)	97.7
Re(3)−O(6)	1.695(9)	1.724	O(6)−Re(3)−F(8)	160.8(4)	159.3
F(7)−Re(3)−F(9)	81.9(4)	81.9	O(5)−Re(3)−F(9)	97.6(4)	98.2
O(6)−Re(3)−F(9)	94.7(4)	92.2	F(8)−Re(3)−F(9)	82.7(3)	84.6
F(7)−Re(3)−F(10)	80.4(4)	80.4	O(5)−Re(3)−F(10)	98.1(4)	98.8
O(6)−Re(3)−F(10)	94.6(4)	91.6	F(8)−Re(3)−F(10)	82.4(3)	85.3
F(9)−Re(3)−F(10)	159.2(3)	161.2			

$ReO_2F_3(CH_3CN)$[e]

Bond Lengths (Å) and Angles (deg)

	LDFT/DZVP		LDFT/DZVP		LDFT/DZVP
Re−O_t	1.715	O_t−Re−O_c	105.5	O_t−Re−$F_{c,c}$	99.1
Re−O_c	1.723	O_t−Re−$F_{c,t}$	100.1	O_t−Re−$F_{c,c}$	99.1
Re−$F_{c,c}$	1.880	O_t−Re−N	174.3	O_c−Re−$F_{c,c}$	93.4
Re−$F_{c,t}$	1.949	O_c−Re−$F_{c,t}$	154.3	O_c−Re−$F_{c,c}$	93.8
Re−$F_{c,c}$	1.873	O_c−Re−N	80.2	$F_{c,c}$−Re−$F_{c,c}$	157.9
Re−N	2.316	$F_{c,c}$−Re−$F_{c,t}$	82.0	$F_{c,c}$−Re−N	79.5
N≡C	1.164	N−Re−$F_{c,c}$	81.1	N−Re−$F_{c,t}$	74.2
$F_{c,c}$−Re−$F_{c,t}$	82.5	Re−N≡C	171.8		

Table 2 (Continued)

$ReO_3F(CH_3CN)_2 \cdot CH_3CN$

Bond Lengths (Å) and Corresponding Bond Valences (vu)[a]

	Re(1)−F(1)	Re(1)−O(1)	Re(1)−O(2)	Re(1)−N(1)
bond valence	0.888	1.837	1.468	0.531
bond length	1.880(5)	1.705(4)	1.788(5)	2.294(4)
tot. bond valence	Re(1): 7.09			

Angles (deg)

O(1)−Re(1)−O(1A)	104.8(3)	O(2)−Re(1)−N(1)	81.5(2)	O(1)−Re(1)−O(2)	99.4(2)	F(1)−Re(1)−N(1)	76.6(2)
O(1)−Re(1)−F(1)	97.8(2)	N(1)−Re(1)−N(1A)	77.9(2)	O(1)−Re(1)−N(1)	88.5(2)	Re(1)−N(1)−C(1)	178.6(5)
O(1)−Re(1)−N(1A)	166.2(2)	N(1)−C(1)−C(2)	178.9(5)	O(2)−Re(1)−F(1)	151.7(2)		

[a] Bond valence units (vu) are defined in ref 33. $R_0 = 1.930$ (Re(VII)═O), $R_0 = 1.836$ (Re(VII)−F), $R_0 = 1.360$ (Li−F), $R_0 = 1.992$ (K−F), $R_0 = 2.132$ (K−O), $R_0 = 2.33$ (Cs−F), $R_0 = 2.06$ (Re−N), and $B = 0.37$ were used (Brown, I. D. Department of Physics, McMaster University, Hamilton, Ontario L8S 4M1, Canada, private communication). [b] Values in parentheses refer to $[K][Re_2O_4F_7]$ in $[K][Re_2O_4F_7]\cdot 2ReO_2F_3$. [c] Experimental values for $(ReO_2F_3)_\infty$ in $[K][Re_2O_4F_7]\cdot 2ReO_2F_3$. [d] Calculated values for monomeric ReO_2F_3 taken from ref 7. [e] The labeling scheme used is defined in structure II. Other observed bond lengths (Å) and bond angles (deg): N−C, 1.136(7); C−C, 1.451(7); C−H, 1.106; C−H, 1.106; C−H, 1.105; N≡C−C, 178.9(9); C−C−H, 109.8; C−C−H, 109.5; C−C−H, 110.3; H−C−H, 108.9; H−C−H, 109.2; H−C−H, 109.1.

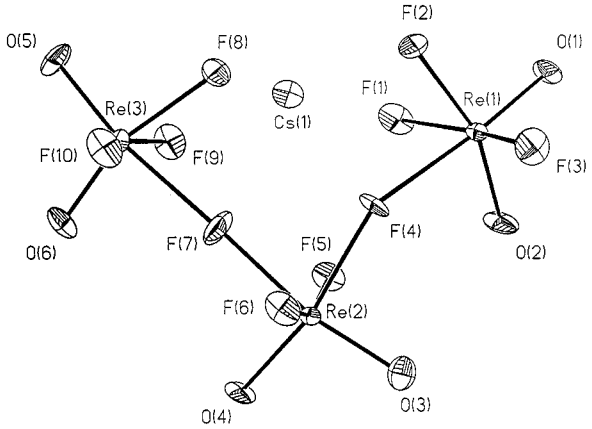

Figure 5. Geometry of the $Re_3O_6F_{10}^-$ anion in $[Cs][Re_3O_6F_{10}]$. Thermal ellipsoids are shown at the 50% probability level.

contacts (2.04(3)−2.108(7) Å) is significantly less than 1 (0.90 vu), the shortest Li···O distance (3.44(3) Å) and the next shortest Li···F distance (3.45(3) Å) are too long to be considered as contacts (the corresponding bond valences are less than 0.01); the shortest Li···Re(1) distance is 3.20(3) Å and is also too long to be a contact.

The potassium cation in $[K][Re_2O_4F_7]$ forms eight long contacts with two anions, six contacts with terminal fluorine atoms (2.711(8), 2.728(9), and 2.820(8) Å) and two contacts with oxygen atoms cis to the fluorine bridge (2.922(9) Å). The total bond valence for K^+ is 1.01 vu. The bond valence values for the light atoms are reasonable except for F(3) (1.15 vu), which is slightly overbonded, and O(2) (1.55 vu), which is underbonded. There are two longer contacts with the bridging fluorine (3.168(7) Å).

The cesium ion in $[Cs][Re_3O_6F_{10}]$ forms six Cs···F contacts with the terminal fluorine atoms of three anions (3.013(7)−3.122(7) Å) providing a total bond valence of 0.94 vu for Cs(1). The next longest contacts are also with terminal fluorine atoms, namely, F(2), 3.194(7), and F(2A), 3.145(8) Å, and with one of the bridging fluorine atoms, F(4), 3.190(7) Å.

The central Re atom in all four compounds is coordinated to two oxygen atoms and four fluorine atoms in which the oxygen atoms are cis to one another providing a distorted octahedral environment around the Re atom. The preference for the *cis*-dioxo-bonded structure is well documented in other *cis*-dioxo species, namely, isoelectronic $WO_2F_4^{2-}$ [36] and OsO_2F_4,[20] the [*cis*-OsO_2F_3] units in the $Os_2O_4F_7^+$ [7] cation, the $TcO_2F_4^-$,[24] $MoO_2F_4^{2-}$,[37] $VO_2F_4^{3-}$,[38] and $ReO_2(OTeF_5)_4^-$ [12] anions, the [*cis*-MO_2F_4] units of the infinite chain species TcO_2F_3,[9] $MoO_2F_3^-$,[39] and $VO_2F_3^-$,[13] and $MoO_2F_2(bpy)$[40] and $WO_2F_2(bpy)$[41] and can be understood in terms of the relative spatial orientations of the strong π-donor oxygen p-orbitals and the empty d_{xy}, d_{xz}, and d_{yz} (approximately $d_{t_{2g}}$) orbitals of the d^0 metal required for $p_\pi \rightarrow d_\pi$ bonding.[24]

The $Re_2O_4F_7^-$ anion consists of two symmetry-related, fluorine-bridged $[ReO_2F_4]$ units, while the structure of the $Re_3O_6F_{10}^-$ anion is an open chain with the central bridging *cis*-ReO_2F_4 unit linked to the Re atom of two terminal ReO_2F_3 groups by bridging fluorine atoms that are cis to one another. The structure of ReO_2F_3 consists of an infinite chain of *cis*-fluorine bridged $[ReO_2F_4]$ units running parallel to the *b*-axis.

The bond lengths of all three anions can be classified into five groups: Re−O_t bonds, trans to Re−F_b bridging bonds; Re−O_c bonds, cis to Re−O_t bonds and trans to terminal fluorines, $F_{c,t}$; Re−$F_{c,c}$ bonds, cis to Re−O_t and Re−O_c bonds and trans to one another; terminal Re−$F_{c,t}$ bonds, cis to Re−O_t bonds and trans to Re−O_c bonds; bridging Re−F_b bonds, trans to Re−O_t bonds.

The Re−O bond lengths are comparable to those in other pseudooctahedral Re(VII) compounds, i.e., $ReOF_5$ (1.64(4) Å),[42] $ReO(OTeF_5)_5$ (1.68(1) Å),[43] Re_2O_7 (1.65(3)−1.73(3) Å),[44] $ReO_2(OTeF_5)_4^-$ (1.664(9) Å),[12] and $ReO_3Cl_3^{2-}$ (1.704(17) Å),[45] and to that of the pentagonal bipyramidal $ReOF_6^-$ anion (1.629(14)−1.671(7) Å)[46] and are longer than the Re(VII)−O bonds in the $Re_2O_2F_9^+$ cation (1.63(2) Å)[18] and the Re(VI)−O double bond in $ReO(OTeF_5)_4\cdot F_2Te(OTeF_5)_2$ (1.63(7) Å).[43] In $Re_2O_4F_7^-$, the Re−O_c bond length 1.753(9) (1.766(7)) Å is found to be considerably longer than the Re−O_t bond length 1.663(12) (1.670(8)) Å. This trend has also been observed in and discussed

(36) Chaminade, J. P.; Moutou, J. M.; Villeneuve, G.; Couzi, M.; Pouchard, M.; Hagenmuller, P. *J. Solid State Chem.* **1986**, *65*, 27.
(37) Grandjean, D.; Weiss, R. *Bull. Soc. Chim. Fr.* **1967**, No. 549, 3049.
(38) Leimkühler, M.; Mattes, R. *J. Solid State Chem.* **1986**, *65*, 260.
(39) Mattes, R.; Müller, G.; Becher, H. J. *Z. Anorg. Allg. Chem.* **1972**, *389*, 177.
(40) Sens, I.; Stenger, H.; Müller, J.; Dehnicke, K. *Z. Anorg. Allg. Chem.* **1992**, *610*, 117.
(41) Arnaudet, L.; Bougon, R.; Bau, R.; Charpin, P.; Isabey, J.; Lance, M.; Nierlich, M.; Vigner, J. *Can. J. Chem.* **1990**, *68*, 507.
(42) Alekseichuk, I. S.; Ugarov, V. V.; Sokolov, V. B.; Rambidi, N. G. *Zh. Strukt. Khim.* **1981**, *22*, 182.
(43) Turowsky, L.; Seppelt, K. *Z. Anorg. Allg. Chem.* **1990**, *590*, 37.
(44) Krebs, B.; Muller, A.; Beyer, H. H. *Inorg. Chem.* **1969**, *8*, 436.
(45) Lis, T. *Acta Crystallogr.* **1983**, *C39*, 961.
(46) Giese, S.; Seppelt, K. *Angew. Chem., Int. Ed. Engl.* **1994**, *33*, 461.

Table 3. Experimental and Calculated Raman Frequencies, Assignments, and Mode Descriptions for $ReO_2F_4^-$

frequencies (cm^{-1})							
expt[a]					DZVP2[b]		
Li^c	$Na^{c,d}$	$K^{d,e}$	$Cs^{c,d,f}$	$N(CH_3)_4^{c,g}$	LDFT	NLDFT	assgnts C_{2v} point sym
1011 (100)	1011 (100) [1005]	987, s [991]	973 (100) [983]	972 (100)	945 (106)	936 (111)	$\nu_1(A_1)$, $\nu_{sym}(ReO_2)$
1004 (4), sh	1005 (4), sh						
998 (2), sh	997 (1), sh						
	983 (9)						
984 (3)	981 (8), sh						
			949 (16), sh	947 (20)[h]			
973 (20)	973 (25) [975]	951, m [958]	939 (16) [946]	939 (19)	920 (203)	917 (200)	$\nu_9(B_1)$, $\nu_{as}(ReO_2)$
962 (2)	964 (<1)						
661 (10)	664 (8) [650]	649, m [645]	649 (5), sh [637]	636 (8)	630 (81)	584 (93)	$\nu_2(A_1)$, $\nu_{sym}(ReF_{2c,c} + ReF_{2c,t})$
640 (1)	648 (1) [624]	606, vvw [609]	634 (8) [608]	605 (1), sh	619 (246)	552 (221)	$\nu_{13}(B_2)$, $\nu_{as}(ReF_{2c,c})$
523 (1)	525 (1) [507]	525, s [523]	535 (1), br [536]	538 (1)	565 (75)	506 (43)	$\nu_3(A_1)$, $\nu_{sym}(ReF_{2c,c} - ReF_{2c,t})$
	[453]	489, s [488]	503 (<1), br [500]	502 (1)	546 (88)	502 (80)	$\nu_{10}(B_1)$, $\nu_{as}(ReF_{2c,t})$
406 (7)	407 (7)	410, m	405 (8), sh	419 (2), sh	363 (8)	361 (2)	$\nu_4(A_1)$, $\delta_{sciss}(ReO_2)$
400 (4), sh	392 (1), sh		398 (11)	402 (8)			
			381 (3)				
344 (3), sh	340 (2), sh			344 (4), sh			$\nu_5(A_1)$, sym comb of *cis*- and
332 (41)	326 (12)	325, s	326 (28)	318 (16)	264 (13)	310 (18)	*trans*-ReF_2 scissor
320 (6)			318 (13)	309 (9), sh	273 (31)	287 (31)	$\nu_{11}(B_1)$, sym comb of $OReF_{c,t}$ sciss
							and $ReF_{2c,c}$ sciss
	280 (1)	278, m	292 (1), sh	293 (2), sh	333 (34)	334 (14)	$\nu_{14}(B_2)$, $\delta_{rock}(ReF_{2c,c}) + \delta_{rock}(ReO_2)$
253 (1)	258 (1)		229 (1), br	223 (>0)	324 (0)	321 (0)	$\nu_7(A_2)$, $ReO_2 + ReF_{2c,t}$ torsion
245 (2)			203 (1), br	192 (1)	287 (29)	242 (58)	$\nu_{15}(B_2)$, $\delta_{rock}(ReF_{2c,t})$
	184 (2), sh						$\nu_6(A_1)$, antisym comb of *cis*- and
177 (23)	173 (5)	180, m	157 (4), br	164 (2)	183 (0)	220 (12)	*trans*-ReF_2 scissor
115 (1)	97 (2)	115, vvw		145 (5)	165 (0)	83 (0)	$\nu_{12}(B_1)$, antisym comb of scissor
110 (2)							$ReOF_{c,t}-ReF_{2c,c}$
83 (2)	79 (3)			75 (>0), sh	167 (0)	109 (0)	$\nu_8(A_2)$, $ReF_{2c,t}-ReO_2$ torsion
76 (1)				47 (2)			lattice vibration

[a] Spectra recorded on a single randomly orientated crystal in a Lindemann capillary (Li^+) and on microcrystalline solids (Na^+, Cs^+, $N(CH_3)_4^+$) in rotating Pyrex glass capillaries at 23 °C using 514.5-nm excitation. Values in parentheses denote relative Raman intensities. Symbols denote the following: shoulder (sh), broad (br), strong band (s), weak (w), medium (m), and very very weak (vvw). Other weak unassigned peaks were observed for $[Li][ReO_2F_4]$ at 947 (1), 937 (1), and 917 (1) cm^{-1}; $[Na][ReO_2F_4]$ at 945 (<1), 937 (<1), and 914 (<1) cm^{-1}; $[Cs][ReO_2F_4]$ at 766 (<1), 884 (2), 902 (2), and 1010 (<1) cm^{-1}; and $[N(CH_3)_4][ReO_2F_4]$ at 837 (1) and 779 (2) cm^{-1}. [b] Infrared intensities, in km mol^{-1}, are given in parentheses. [c] Unbracketed values are from this work. [d] Values given in brackets are infrared frequencies obtained from ref 26. [e] Unbracketed values are Raman frequencies and intensities from ref 10 except unbracketed values for ν_3 and ν_{10}, which are infrared frequencies from ref 10. [f] The spectrum of $[Cs][ReO_2F_4]$ was also recorded in HF solution (1.0 g/mL of HF) in an FEP sample tube with bands at 1002 (100, p), $\nu_1(A_1)$; 972 (51, dp), $\nu_9(B_1)$; 654 (18, dp), $\nu_2(A_1)$; 402 (42, p), $\nu_4(A_1)$; 327 (41, p), $\nu_5(A_1)$; and 293 (24), $\nu_4(B_2)$, overlaps with an FEP line, 209 (2), $\nu_{15}(B_2)$, and 168 (5), $\nu_6(A_1)$ cm^{-1}. Bands arising from the FEP sample tube were observed at 293 (24), 386 (22), 576 (3), 599 (3), 733 (50), and 751 (6) cm^{-1}. The symbols denote the following: polarized (p) and depolarized (dp). [g] The $N(CH_3)_4^+$ cation modes were observed at 374 (4), $\nu_8(E)$; 459 (8), $\nu_9(T_2)$; 742 (8, sh); 752 (13), $\nu_3(A_1)$; 1177 (2), $\nu_7(E)$; 1287 (1), $\nu_{17}(T_2)$; 1418 (3), $\nu_{16}(T_2)$; 1450 (1, sh), 1463 (8), 1468 (9), $\nu_2(A_1)$; and 2823 (4), 2887 (2, sh), 2929 (8), 2968 (11), 2993 (8), 3041 (16), $\nu_5(E)$ cm^{-1} (see ref 55). [h] This band overlaps with $\nu_{18}(T_2)$ of $N(CH_3)_4^+$.

for the isoelectronic $Os_2O_4F_7^+$ cation ($Os-O_c$ (1.750 Å) > $Os-O_t$ (1.676 Å)).[7] The difference is presumably enhanced in the present structure by significant interaction with K^+ at 2.97(1) (2.925(8)) Å and long contacts between F atoms of neighboring anions with the O_c atom, whereas no such interactions exist for the O_t atom. This trend is also observed in $Re_3O_6F_{10}^-$ for the two $Re-O_t$ and $Re-O_c$ bond lengths associated with the terminal rhenium atoms (Table 3), whereas the two central $Re-O_t$ bond lengths are equal within experimental error (3σ). The Re−O bond lengths are generally shorter than the Os−O bond lengths in the $Os_2O_4F_7^+$ cation.[7] The d orbitals in all three rhenium anions and polymeric ReO_2F_3 are expected to be less contracted and, hence, more available for $p_\pi-d_\pi$ interactions between ligand filled 2p orbitals and empty metal d_{xy}, d_{xz}, and d_{yz} orbitals than they are in the Os(VIII) cation, $Os_2O_4F_7^+$, which contains a more electronegative metal center.

The $Re-F_{c,c}$ and $Re-F_{c,t}$ bond distances of all three anions and of polymeric ReO_2F_3 are generally in good agreement with the terminal Re−F bond distances in ReO_3F (1.859(8) Å),[47] $ReOF_6^-$ (ax, 1.894(11)−1.927(10); eq, 1.862(2)−1.917(7) Å),[46] $ReOF_5$ (1.810(7) Å),[42] ReO_2F_3 (calculated: ax, 1.876; eq, 1.894 Å),[7] $(ReOF_4{\cdot}SbF_5)_2$ (1.841(15) Å),[48] and $ReOF_4$ (1.86(4) Å),[15] except in $ReO_2F_4^-$ where the $Re-F_{c,t}$ bond distance is in better agreement with the $Re-F_b$ bond distances in $ReOF_4$ (2.14(4) Å; range, 1.99(4)−2.28(4) Å)[15] and in $Re_2O_2F_9^+$ (2.060(4) Å).[18] In both $ReO_2F_4^-$ and $Re_3O_6F_{10}^-$, the $Re-F_{c,t}$ bonds trans to the oxygen atoms are significantly longer than the $Re-F_{c,c}$ bonds trans to fluorine atoms, a feature in common with OsO_2F_4,[20] $TcO_2F_4^-$,[24] the $[OsO_3F_3]$, $[TcO_2F_4]$, and $[MoOF_5]$ units of the infinite chain polymers OsO_3F_2,[49] TcO_2F_3,[9] and $MoOF_4$,[14] the $[TcOF_5]$ unit of trimeric $TcOF_4$,[16] and the [*cis*-OsO_2F_4] unit of $Os_2O_4F_7^+$.[7] The difference has been attributed to the trans influence of the M−O double bonds of the d^0 metal, for which there are significant $p_\pi \rightarrow d_\pi$ interactions.[7,9,24] As a consequence, the $M-F_{c,t}$ bond lengths resemble those of $M-F_b$ bonds.

The $Re-F_{c,c}$ and $Re-F_{c,t}$ bonds are also longer and more polar than the corresponding $Os-F_c$ and $Os-F_t$ bonds in the $Os_2O_4F_7^+$ cation[7] and in neutral OsO_2F_4[20] whereas the Re−O bonds are somewhat shorter than the Os−O bond lengths of the aforementioned Os(VIII) oxide fluorides. The polarities of the metal−fluorine σ-bonds are expected to be more affected

(47) Lotspeich, J. F.; Javan, A. *J. Chem. Phys.* **1959**, *31*, 633.
(48) Fawcett, J.; Holloway, J. H.; Russell, D. R. *J. Chem. Soc., Dalton Trans.* **1981**, 1212.
(49) Bougon, R.; Buu, B.; Seppelt, K. *Chem. Ber.* **1993**, *126*, 1331.

by charge than the metal−oxygen π-bonds. We also note that the Re−F bond lengths are also influenced by interactions of the F atoms with the M^+ cations (see Computational Results).

The Re−F_b bond distance in $Re_2O_4F_7^-$ (2.150(3) Å) is comparable to those in $[Cs][Re_3O_6F_{10}]$ (2.213(9)−2.148(8) Å), and the bridging angle of 143.3(6)° is very similar to that in $[H_3O][W_2O_2F_9]$[19] (144(2)°) and approaches the ideal value for hexagonal close packing of the light atoms (132°).[17]

The Re−F_b bond distances in $Re_3O_6F_{10}^-$ are asymmetric with average Re−F_b bond distances around the central rhenium, Re(2) (2.061(8)−2.042(6) Å), comparable to those observed in the $ReO_2F_4^-$ anion (2.001(6) Å) and in $(ReOF_4{\cdot}SbF_5)_2$ (2.079(15) Å; Re−F_b trans to a terminal fluorine)[48] but shorter than those around the terminal rhenium atoms, Re(1) and Re(3) (2.213(9)−2.148(8) Å). The Re−F_b bond lengths associated with the terminal rhenium atoms are similar to those of the Re−F_b bonds (2.231(15) Å) in $(ReOF_4{\cdot}SbF_5)_2$,[48] which are also trans to Re−O bonds. The asymmetry among the Re−F_b bond lengths is reflected in their bond valence values (Table 2). As the number of terminal fluorine atoms varies from 2 for the central rhenium atom to 3 for the terminal rhenium atoms, the rhenium bond valence sum must remain constant at or near 7 so that the bridge must elongate to partially compensate for the bond valence contribution of the additional terminal fluorine on each terminal rhenium atom. The difference between the two bridging bond lengths, Re(1)−F(4) and Re(3)−F(7), is attributed to the long F(4)···Cs(1) contact which serves to elongate the Re(1)−F(4) bond.

The terminal Re−$F_{c,c}$ bond distances in $(ReO_2F_3)_\infty$ (average: 1.844(7) Å) are slightly shorter than in $[Li][ReO_2F_4]$, and the Re−F_b bond (average: 2.102(6) Å) is longer than Re−$F_{c,c}$, as expected for a bridging fluorine. The bridging angle between each ReO_2F_4 unit is 156.0(4)° and is slightly larger than that observed in TcO_2F_3 (148.8(3)°).[9]

The bond valence sum for each rhenium atom is very close to 7 vu in all four structures (Table 2), indicating that all significant contacts to the rhenium atoms have been accounted for. The bond valence values of the Re−O and Re−F in $(ReO_2F_3)_\infty$ are very close to the ideal values of 1 for the terminal fluorines, 2 for the oxygens, and 0.5 for the bridging fluorine atom. The differences observed among the anions result from long contacts between selected F or O atoms and the alkali metals which contribute to the bond valence sum to the extent required to fulfill the valence requirements of each Re atom (Table 2). This is supported by the two Re−F_b−Re bond angles in $Re_3O_6F_{10}^-$, Re(1)−F(4)−Re(2) and Re(2)−F(7)−Re(3), which differ by almost 40°. The Re(2)−F(7)−Re(3) angle is essentially linear (178.7(6)°), close to the ideal angle for cubic close packing (180°),[17] and the corresponding long contact to F(7) is Cs(1)−F(7), 3.749(11) Å, whereas the Re(1)−F(4)−Re(2) angle is 140.5(4)°, approaching the ideal value for hexagonal close packing (132°).[17] The Cs(1)−F(4) contact is shorter, 3.189(7) Å, and in this case, the distortion permits a contact between Cs(1) and F(4) which allows the ideal bond valence for F(4) to be achieved.

Although there is considerable variation in the bond lengths around the rhenium atom, the octahedra formed by the light atoms are relatively undistorted, as shown by the average interligand atom distances which are all within the range 2.47(1)−2.72(1) Å. The average values of the angles in $Re_2O_4F_7^-$, $Re_3O_6F_{10}^-$, and $(ReO_2F_3)_\infty$ are very similar to those found in $ReO_2F_4^-$ (Table 2). The asymmetry of the distortion is also reflected in the angles the light atoms subtend with the rhenium atom(s) and has been rationalized in terms of the VSEPR model of molecular geometry[50] in the infinite chain polymer TcO_2F_3[9] and the structurally related $Os_2O_4F_7^+$ cation[7] and $TcO_2F_4^-$ anion.[24]

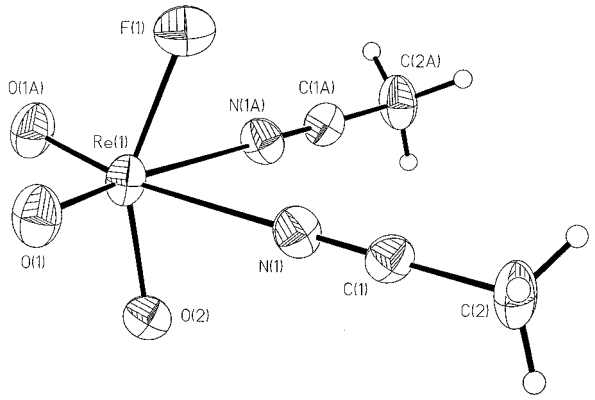

Figure 6. Geometry of $ReO_3F(CH_3CN)_2{\cdot}CH_3CN$. Thermal ellipsoids are shown at the 50% probability level.

$ReO_3F(CH_3CN)_2{\cdot}CH_3CN$. In an attempt to grow crystals of $ReO_2F_3(CH_3CN)$, single crystals of the hydrolysis product, $ReO_3F(CH_3CN)_2{\cdot}CH_3CN$ (Figure 6), were obtained. The coordination around the Re atom comprises a pseudooctahedral arrangement of three oxygen atoms, a fluorine atom, and two nitrogen-coordinated CH_3CN molecules. The oxygen atoms adopt a facial arrangement, which results in the coordination of the fluorine atom and each CH_3CN ligand trans to an oxygen atom. The *fac*-isomer is expected to be more stable than the *mer*-isomer because each filled p orbital on an oxygen competes equally for the three available empty $d_{t_{2g}}$ orbitals on the rhenium in the *fac*-isomer rendering it more stable. Similar arguments are used to account for the *cis*-dioxo arrangements described earlier in this paper. Other examples of octahedral oxide halide anions that have facial arrangements include $MoO_3F_3^{3-}$,[51] $ReO_3Cl_3^{2-}$,[45] and $OsO_3F_3^-$.[52]

The Re atom is found to lie below the [O(1), O(1A), N(1), N(1A)] plane by 0.054 Å toward F(1) as a result of the greater repulsion between the larger Re═O bond pair domain and the bond pair domains of the neighboring ligands. The lengths of the Re−O bonds trans to the CH_3CN ligands (1.704(3) Å) are comparable to other Re(VII)−O bonds. As expected, the Re−O_t bond trans to the F atom is significantly longer (1.801(6) Å) than the Re−O_c bond and is even longer than the Re−O_c bond in $[K][Re_2O_4F_7]$. The Re−F(1) bond length (1.883(5) Å) is also affected by the trans influence of the oxo ligand and is intermediate between the Re−$F_{c,c}$ and Re−$F_{c,t}$ bond lengths observed in the related oxo compounds (*vide supra*). The Re−N bond length, as well as the geometric parameters for CH_3CN, is similar to other d^0 transition metal complexes with CH_3CN (e.g., $[ReO_2(CH_3CN)_3][ReO_4]$,[53] Re−N, 2.267(2)−2.289(3) Å, and (η^2-CH_3CO_2)$ReO_3(CH_3CN)$, Re−N, 2.331(5) Å, N−C, 1.111(8) Å, and C−C, 1.452(9) Å).[53] The O−Re−O angle (104.8(3)°) is significantly larger than 90° while the N−Re−N (77.9(2)°) angle is smaller and is presumably the result of the larger oxygen bond pair domains.

When viewed along the *b*-axis, the extended structure of $ReO_3F(CH_3CN)_2$ shows that within an *ab*-plane each molecule

(50) Gillespie, R. J.; Hargittai, I. *The VSEPR Model of Molecular Geometry*; Allyn and Bacon: Boston, MA, 1991.
(51) Griffith, W. P. *J. Chem. Soc. A* **1969**, 211.
(52) Jones, P. J.; Levason, W.; Tajik, M. *J. Fluorine Chem.* **1984**, *25*, 195.
(53) Herrmann, W. A.; Roesky, P. W.; Kühn, F. E.; Elison, M.; Artus, G.; Scherer, W.; Romao, C. C.; Lopes, A.; Basset, J.-M. *Inorg. Chem.* **1995**, *34*, 4701.

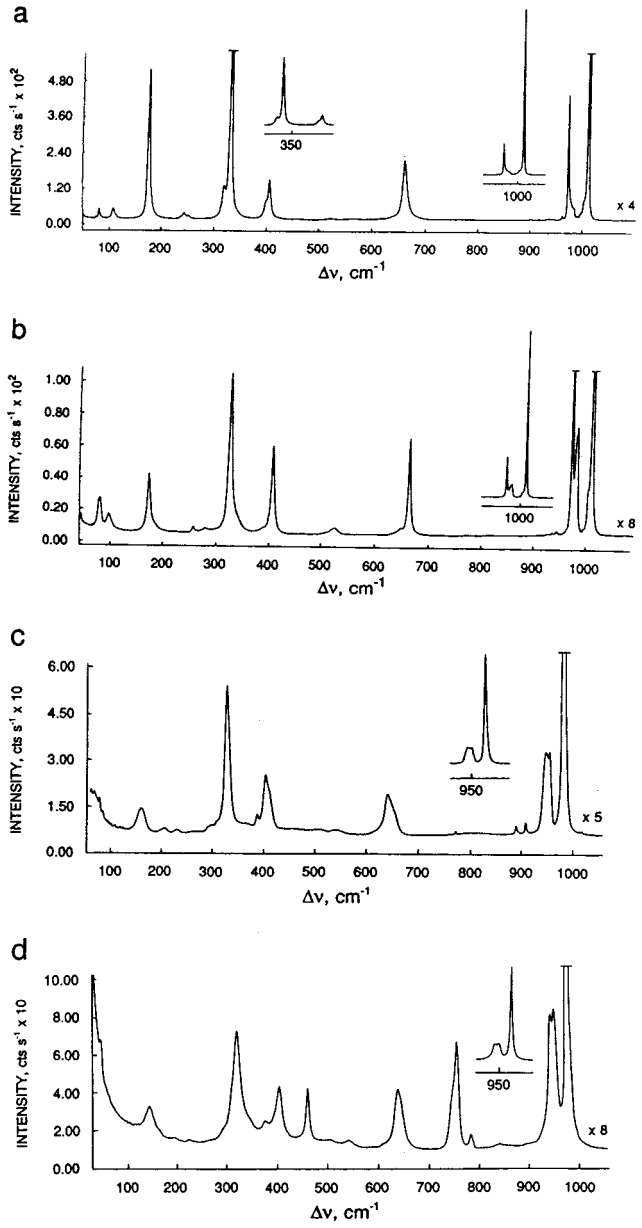

Figure 7. Raman spectra of microcrystalline (a) $[Li][ReO_2F_4]$, (b) $[Na][ReO_2F_4]$, (c) $[Cs][ReO_2F_4]$, and (d) the low-frequency range of $[N(CH_3)_4][ReO_2F_4]$ recorded in Pyrex capillaries at 22 °C using 514.5-nm excitation.

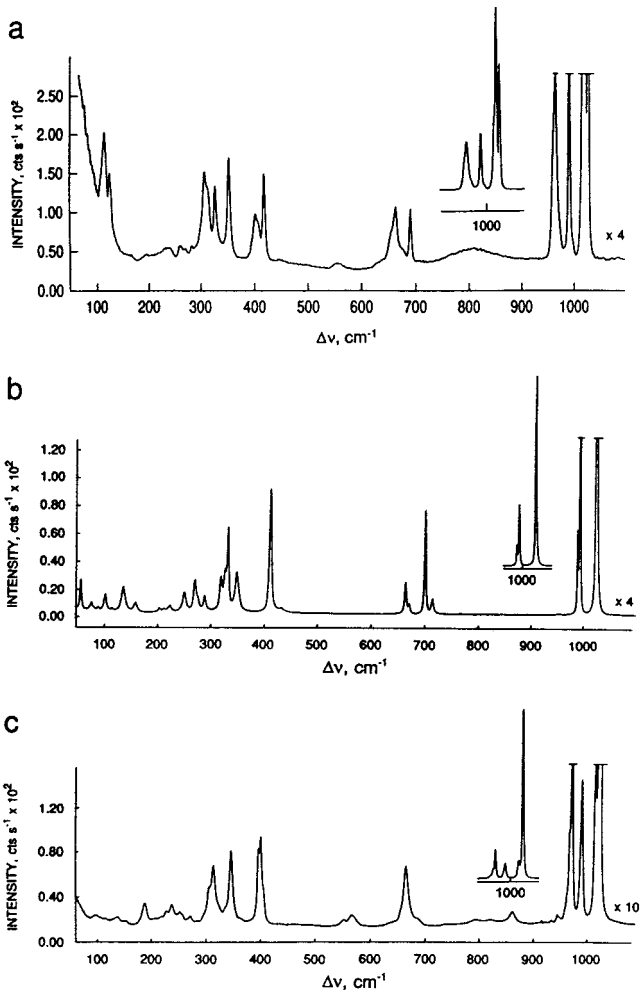

Figure 8. Raman spectra of microcrystalline (a) $[K][Re_2O_4F_7]\cdot 2ReO_2F_3$, (b) ReO_2F_3, and (c) $[Cs][Re_3O_6F_{10}]$ recorded in Pyrex capillaries at 22 °C using 514.5-nm excitation.

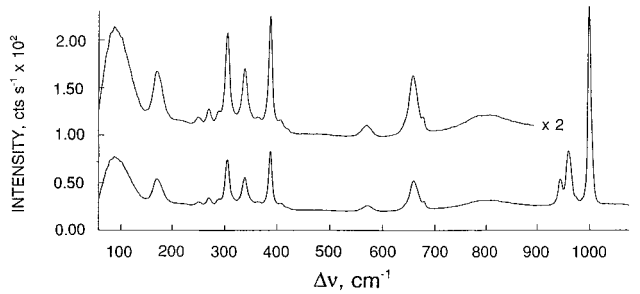

Figure 9. Raman spectrum (low-frequency range) of microcrystalline $ReO_2F_3(CH_3CN)$ recorded in a Pyrex capillary at 23 °C using 514.5-nm excitation.

is rotated 90° with respect to its nearest neighbor, and each molecule is rotated 180° relative to its nearest neighbor in an adjacent plane. This arrangement results in large channels that run in the *b*-direction and which contain disordered CH_3CN solvent molecules.

Raman Spectroscopy and Vibrational Assignments of $[M][ReO_2F_4]$ [M = Li, Na, Cs, $N(CH_3)_4$], $(ReO_2F_3)_\infty$, $ReO_2F_3(CH_3CN)$, $[K][Re_2O_4F_7]$, $[K][Re_2O_4F_7]\cdot 2ReO_2F_3$, and $[Cs][Re_3O_6F_{10}]$. The spectra are reproduced in Figures 7−9, and the assignments are summarized in Tables 3−5 along with their theoretical values. With the exception of $[Cs][Re_3O_6F_{10}]$ and $(ReO_2F_3)_\infty$, the assignments of the observed Raman vibrational frequencies were aided by LDFT and NLDFT calculations. The experimental and calculated vibrational frequencies for monomeric ReO_2F_3 and their assignments have been previously discussed[7] and were also used to aid in the vibrational assignments of the related anions, adducts, and $(ReO_2F_3)_\infty$.

Vibrational activities of the anions in $[Li][ReO_2F_4]$, $[K][Re_2O_4F_7]$, $[K][Re_2O_4F_7]\cdot 2ReO_2F_3$, and $[Cs][Re_3O_6F_{10}]$ and of $(ReO_2F_3)_\infty$ in $[K][Re_2O_4F_7]\cdot 2ReO_2F_3$ have been determined in their respective unit cells by correlation of the gas-phase symmetries to the crystallographic anion site and unit cell symmetries.[54] The $ReO_2F_4^-$ anion (C_{2v}), when correlated with the anion site symmetry C_{2v} and the crystal symmetry D_{2d}, is predicted to have all modes Raman and infrared active with only $\nu_1-\nu_6$ split into A_1 and B_2 components in the Raman spectrum. The factor-group analysis for $ReO_2F_4^-$ is valid for both the Li^+ and Na^+ salts, which were shown to be isostruc-

(54) Carter, R. J. *J. Chem. Educ.* **1971**, *48*, 297 and references therein.

Table 4. Experimental Raman Frequencies, Assignments, Mode Descriptions for $[K][Re_2O_4F_7]$, $[K][Re_2O_4F_7]\cdot 2ReO_2F_3$, $[Cs][Re_3O_6F_{10}]$, and Polymeric ReO_2F_3 and Calculated Frequencies for $Re_2O_4F_7^-$

$Re_2O_4F_7^-$ frequency, cm^{-1}				$Re_3O_6F_{10}^-$ frequency, cm^{-1}	assgnt for the $Re_cO_2F_4$ unit in	ReO_2F_3 frequency, cm^{-1}	
$[K][Re_2O_4F_7]$[a,b]	$[K][Re_2O_4F_7]\cdot 2ReO_2F_3$[a–c]	calc[d]	assgnt in C_2 point sym[e]	$[Cs][Re_3O_6F_{10}]$[a,b,f,g]	C_{2v} point sym[e]	$(ReO_2F_3)_\infty$[a,h]	$[K][Re_2O_4F_7]\cdot 2ReO_2F_3$[a–c]
				1024 (100), Re_c	A_1, $\nu_{sym}(Re_cO_2)$	1025 (100)	[1028 (65)]
				1016 (11), Re_c			[1021 (100)]
							[1017 (38), sh]
983 (11)	[995 (3), sh]	983 (10)	A, $\nu_s[(Re_tO_t + Re_tO_c) + (Re_t'O_t + Re_t'O_c)]$	972 (16), Re_t			
	[990 (28)]	977 (218)	B, $\nu_s[(Re_tO_t + Re_tO_c) - (Re_t'O_t + Re_t'O_c)]$				
				990 (9), Re_c	B_1, $\nu_{as}(Re_cO_2)$	994 (33)	992 (29)
						990 (11)	
966 (88)	[968 (6), sh]	948 (178)	A, $\nu_{as}[(Re_tO_t - Re_tO_c) + (Re_t'O_t - Re_t'O_c)]$	968 (6), sh Re_t			
960 (9), sh	[961 (24)]	944 (157)	B, $\nu_{as}[(Re_tO_t - Re_tO_c) - (Re_t'O_t - Re_t'O_c)]$				
				688 (<1), Re_c	A_1, $\nu_{sym}(Re_cF_{2c,c})$	713 (2)	
						700 (14)	690 (6)
	[663 (8)]	662 (77)	B, $\nu_s[(Re_tF_{2c,c} + Re_tF_{c,t}) - (Re_t'F_{2c,c} + Re_t'F_{c,t})]$				
653 (4)	654 (4), sh	659 (115)	A, $\nu_s[(Re_tF_{2c,c} + Re_tF_{c,t}) + (Re_t'F_{2c,c} + Re_t'F_{c,t})]$	655 (1), Re_t			
				665 (4), Re_c	B_2, $\nu_{as}(Re_cF_{2c,c})$	670 (1), sh	677 (2), sh
						664 (4)	[663 (8)]
		655 (321)	B, $\nu_{as}[(Re_tF_{2c,c}) + (Re_t'F_{2c,c})]$				
639 (5)	638 (1), br	644 (19)	A, $\nu_{as}[(Re_tF_{2c,c}) - (Re_t'F_{2c,c})]$	641 (<1), Re_t			
		582 (79)	A, $\nu(Re_tF_{c,t} + Re_t'F_{c,t}) - \nu_s(Re_tF_{2c,c} + Re'F_{2c,c})$				
		582 (30)	B, $\nu(Re_tF_{c,t} - Re_t'F_{c,t}) - \nu_s(Re_tF_{2c,c} - Re'F_{2c,c})$				
				568 (<1), Re_c	$\nu_{as}(Re_cF_bRe_t')$		
	554 (1), br	512 (270)	B, $\nu_{as}(Re_tF_bRe_t')$	553 (<1), Re_t			
				405 (3), sh Re_c	A_1, $\delta_{sciss}(Re_cO_2)$	432 (<1)	445 (>0)
						412 (17)	417 (12)
398 (6)	405 (5), sh	383 (1)	A, $\delta_{sciss}(Re_tO_2 + Re_t'O_2)$	400 (6), Re_t			
388 (5)	400 (6)	380 (13)	B, $\delta_{sciss}(Re_tO_2 - Re_t'O_2)$	396 (5)			
				363 (<1)			
349 (91)	[351 (13)]	354 (5)	A, $\delta_{sciss}[(O_cRe_tF_{c,c} + F_{c,c}Re_tF_{c,t}) + (O_cRe'F_{c,c} + F_{c,c}Re'F_{c,t})]$	346 (4)	A_1, sym comb of $Re_cF_{2c,c}$ and Re_cF_{2b}	349 (6)	[351 (13)]
		352 (5)	B, $\delta_{sciss}[(O_cRe_tF_{c,c} + F_{c,c}Re_tF_{c,t}) - (O_cRe'F_{c,c} + F_{c,c}Re'F_{c,t})]$				
337 (100)		335 (2)	B, $\delta(F_{c,c}Re_tF_b - F_{c,c}Re_t'F_b + Re_tF_bRe_t')$				
332 (44)	[326 (9)]	331 (0)	A, $\delta(F_{c,c}Re_tF_b + F_{c,c}Re_t'F_b + Re_tF_bRe_t')$	336 (<1), sh	B_1, sym comb of ORe_cF_b	332 (11)	
		323 (17)	A, $\delta(F_bRe_tO_t + F_bRe_t'O_t + Re_tF_bRe_t')$	321 (<1), sh	sciss and $Re_cF_{2c,c}$	326 (6), sh	[326 (9)]
	[312 (9), sh]	319 (58)	B, $\delta(F_bRe_tO_t - F_bRe_t'O_t + Re_tF_bRe_t')$	313 (4)	sciss	319 (5)	[312 (9), sh]
	305 (11)	314 (7)	A, $O_cF_{2c,c}F_{c,t}Re_t$(inversion) + $O_cF_{2c,c}F_{c,t}Re_t'$(inversion)	307 (3)			
	298 (4), sh			298 (<1), sh			
	[280 (1)]	281 (44)	B, $\delta(F_{c,c}Re_tF_{c,c} - F_{c,c}Re_t'F_{c,c} + Re_tF_bRe_t')$	285 (<1)	B_2, $\delta_{rock}(Re_cF_{2c,c})$	288 (1)	[280 (1)]
						276 (2), sh	
	268 (1)	261 (9)	A, $\delta(F_{c,c}Re_tF_{c,t} + F_{c,c}Re_t'F_{c,t} + Re_tF_bRe_t')$	271 (<1)		270 (5)	
250 (3)	258 (1)	259 (77)	B, $\delta(F_{c,c}Re_tF_{c,t} - F_{c,c}Re_t'F_{c,t} + Re_tF_bRe_t')$	255 (<1), sh		251 (3)	
				250 (1)			
	237 (1), br	223 (8)	B, $\delta(F_{c,t}Re_tF_{c,c} + F_{c,t}Re_t'F_{c,c} + F_{c,c}Re_tO_t + F_{c,c}Re_t'O_t)$	238 (1)			
		222 (8)	A, $\delta[(F_{c,t}Re_tF_{c,c} - F_{c,t}Re_t'F_{c,c}) - (Re_tF_bRe_t' + F_{c,c}Re_t'O_t)]$	228 (<1)	A_2, Re_cO_2 torsion	223 (<1)	229 (1)
				218 (<1), Re_c		213 (<1)	
				205 (<1), Re_c		204 (<1)	
	193 (1)	196 (5)	A, $\delta_{oop}(Re_tOF_3 - Re_t'OF_3)$				
180 (1)		187 (8)	B, $\delta(F_{c,t}Re_tO_c - F_{c,t}Re_t'O_c)$	188 (1), Re_t			
				153 (<1), Re_c		159 (1)	
		139 (0)	A, $Re_tO_2F_3$ rock	138 (<1)		136 (4)	
122 (3)	123 (9)	128 (0)	A, $Re_tO_2F_3$ torsion				
		123 (1)	A, $\delta(O_tRe_tF_b + O_tRe_t'F_b)$				
		117 (2)	B, rock Re_t group − rock Re_t' group[i]				
105 (13)	[112 (9)]	108 (0)	A, $\nu_s(Re_tF_bRe_t')$	114 (<1)	$\nu_s(Re_cF_bRe_t')$	114 (<1)	[112 (9)]
				99 (<1)		101 (2)	
		70 (0)	A, rock Re_t group + rock Re_t' group[j]			87 (<1)	
						75 (1)	
						55 (4)	

Table 4 (Continued)

[a] Values in parentheses denote relative Raman intensities. Symbols denote the following: shoulder (sh) and broad (br). [b] Spectrum recorded on a randomly orientated single crystal in a Lindemann glass capillary at 22 °C using 514.5-nm excitation. [c] Values in square brackets denote coincident bands or bands which cannot be uniquely assigned to either $Re_2O_4F_7^-$ or $(ReO_2F_3)_\infty$ in $[K][Re_2O_4F_7]\cdot 2ReO_2F_3$. A broad, unassigned peak was also observed at 800 (<1) cm^{-1}. [d] Infrared intensities, in km mol^{-1}, are given in parentheses. [e] The labels Re_t and Re_c refer to the terminal and central rhenium atoms, respectively, of $Re_3O_6F_{10}^-$. [f] Where possible, frequency values for the central $Re_cO_2F_4$-group are aligned with those of the $Re_cO_2F_4$-units in $(ReO_2F_3)_\infty$ and frequency values for the terminal $Re_tO_2F_3$-groups are aligned with those of the $Re_2O_4F_7^-$ anion. [g] Several weak, unassigned peaks were also observed at 947 (<1), 934 (<1), 923 (<1), 862 (<1), 822 (<1), and 793 (<1) cm^{-1}. [h] Spectrum recorded on microcrystalline solid in a Pyrex capillary at 22 °C using 514.5-nm excitation. Several weak, unassigned peaks were also observed at 957 (<1) and 952 (<1) cm^{-1}. [i] $\delta(O_tRe_tF_b - O_tRe_t'F_b)$. [j] $\delta(O_tRe_tF_b + O_tRe_t'F_b)$.

Table 5. Experimental and Calculated Raman Frequencies, Assignments, and Mode Descriptions for $ReO_2F_3(CH_3CN)$

frequencies (cm^{-1})			
solid[a,b]	soln[a,c]	calc[d]	assgnts
3016 (3)	*e*	3082 (3)	$\nu_{as}(CH_3)$
		3077 (3)	$\nu_{as}(CH_3)$
2947 (33)	*e*	2989 (5)	$\nu_{sym}(CH_3)$
2323 (22)	2324 (14), p	2373 (113)	$\nu(CN)$
2297 (18)	*e*		
1412 (1)	*e*	1387 (19)	$\delta_{as}(CH_3)$
	e	1381 (20)	$\delta_{as}(CH_3)$
1367 (6)	1366 (7), sh, p	1340 (15)	$\delta_{sym}(CH_3)$
	1041 (1), dp	1028 (118)	$\nu(ReO_t) + \nu(ReO_c)$
1001 (100)	1002 (100), p	1006 (117)	$\nu(ReO_t) - \nu(ReO_c) + \delta_{rock}(CH_3)$
974 (2), sh	974 (4), sh, p	987 (17)	$\delta_{rock}(CH_3) + \nu(ReO_c) + \delta(CCN)$
960 (26)	962 (25), p	976 (19)	$\nu(ReO_c) - \nu(ReN) + \nu(CC) + \delta_{rock}(CH_3)$
944 (13)	943 (15), p	986 (17)	$\delta_{rock}(CH_3) + \nu(CC)$
679 (5), sh		676 (53)	$\nu_{sym}(ReF_{2c,c}) + \nu(ReF_{c,t})$
659 (15)	660 (22), p	667 (155)	$\nu(ReF_{c,t}) - \nu(ReF_{c,c})$
572 (3)	571 (2), dp	560 (57)	$\nu(ReF_{c,t}) - \nu(ReF_{2c,c})$
423 (1)		449 (14)	$\delta(ReO_2) + \delta(CNRe)$
408 (4)	406 (3), sh, dp	408 (6)	$\delta(ReO_2) - \delta(CNRe)$
389 (30)	388 (16), p	401 (8)	$\delta(O_tReN) - \delta(CNRe)$
366 (3)	*e*	383 (3)	$\delta(O_tReF_{c,c}) + \delta(CNRe)$
340 (15)	341 (7), dp	347 (1)	$\delta(O_cReF_{c,c}) + \delta(F_{c,c}ReF_{c,t})$
307 (24)	307 (10), dp	322 (16)	$\delta(F_{c,c}ReO_t) + \delta(F_{c,t}ReF_{c,c}) + \delta(O_cReN)$
292 (4)	290 (2), p		
278 (2), sh			
272 (4)	272 (3), p	262 (17)	$\delta(F_{c,c}ReO_c) + \delta(F_{c,c}ReO_c) - \delta(F_{c,t}ReN)$
257 (2)	253 (2), dp	257 (23)	$\delta(F_{c,c}ReN) + \delta(OcReF_{c,t})$
252 (2)			
		221 (6)	$\nu(ReN) + \delta(F_{c,c}ReF_{c,c})$ toward $F_{c,t}$
		212 (10)	$\nu(ReN) + \delta(F_{c,c}ReF_{c,c})$ toward $F_{c,t}$
188 (8), sh		202 (5)	$\delta(F_{c,c}ReF_{c,c})$ toward N
182 (10), sh		183 (2)	$\delta(NReF_{c,c}-NReF_{c,c})$
174 (11)	171 (7), dp	130 (1)	$\delta(CH_3)-N-(ReO_2F_3)$ plane 1
154 (<1)		114 (2)	$\delta(CH_3)-N-(ReO_2F_3)$ plane 2
90 (23)		81 (6)	$\tau(CH_3)$

[a] Values in parentheses denote relative intensities. Symbols denote the following: shoulder (sh), broad (br), polarized (p), and depolarized (dp). [b] Spectrum recorded on microcrystalline solid in a rotating Pyrex capillary at 23 °C using 514.5-nm excitation. [c] Spectrum recorded in CH_3CN solution in 3-mm o.d. Pyrex tube at 23 °C using 514.5-nm excitation. Frequency values observed for CH_3CN solvent (23 °C): 3004 (3), ν_5(E); 2945 (100), ν_1(A_1); 2735 (2), $2\nu_3$; 2294 (4), $\nu_3 + \nu_4$; 2254 (67), ν_2(A_1); 1447 (<1), ν_6(E); 1375 (3), ν_3(A_1); 918 (16), ν_4(A_1); 379 (5), ν_8(E). [d] Infrared intensities, in $kmol^{-1}$, are given in parentheses. [e] Obscured by a peak from CH_3CN solvent (see footnote *c*).

tural. All modes are both Raman and infrared active for $Re_2O_4F_7^-$ (C_2), but no factor-group splitting is predicted when correlated to the anion site symmetry C_2 and the unit cell symmetry C_{2h} of $[K][Re_2O_4F_7]$. All the bands are Raman and infrared active and are expected to be split in both the Raman ($\nu_1-\nu_{18}$ split into two A components) and infrared spectra ($\nu_{19}-\nu_{33}$ split into two B components) when correlated to the anion site symmetry C_2 and the unit cell symmetry C_2 of $[K][Re_2O_4F_7]\cdot 2ReO_2F_3$. Correlation of the free molecule symmetry of $(ReO_2F_3)_\infty$ (C_s) to the molecule site symmetry (C_1) and the unit cell symmetry (C_2) of $[K][Re_2O_4F_7]\cdot 2ReO_2F_3$ reveals that all the bands are expected to be active and split in both the Raman and infrared spectra into A and B components. Correlation of the free anion symmetry of $Re_3O_6F_{10}^-$ (C_{2v}) to the anion site symmetry (C_1) and the unit cell symmetry (C_i) reveals that all of the bands are Raman and infrared active but are not factor-group split.

[M][ReO_2F_4] [M = Li, Na, Cs, $N(CH_3)_4$]. Assignments were based on a *cis*-$ReO_2F_4^-$ anion having C_{2v} symmetry (see X-ray Crystal Structure of $Li^+ReO_2F_4^-$ and structure I). All 15 vibrational modes having the symmetries $6A_1 + 2A_2 + 4B_1 + 3B_2$ (the [O_c, O_c, Re, $F_{c,t}$, $F_{c,t}$] plane is taken as the $\sigma_v(xz)$-plane with the *z*-axis as the principal axis) are expected to be Raman and infrared active. Assignments were also made by comparison with $TcO_2F_4^-$ [24] and OsO_2F_4[20] for which there are also calculated frequencies.

The present assignments for the $[M][ReO_2F_4]$ [M = Li, Na, Cs, $N(CH_3)_4$] are in agreement with those reported by Yagodin et al.,[26] who only reported the six highest infrared frequencies for the Na^+, K^+, Rb^+, and Cs^+ salts. Kuhlmann and Sawodny[10] reported 14 vibrational modes from a Raman and infrared vibrational study of $[K][ReO_2F_4]$, and their assignments for the first seven modes, $\nu_1-\nu_4$, ν_9, ν_{12}, and ν_{13}, agree with the present assignments. The low-frequency modes have been reassigned in this work and are reported in Table 4. Since no polarization measurements have been reported previously for $ReO_2F_4^-$, the present work also reports polarization measurements for the cesium salt in HF solution.

The splittings observed for the A_1 modes, ν_1, ν_4, ν_5, and ν_6, of the Li^+ and Na^+ salts are in agreement with the factor-group analyses. The additional splitting observed for $\nu_1(A_1)$ likely results from a Fermi resonance between a combination of the totally symmetric $\delta(ReF_{2c,c})$, $\nu_2(A_1)$, and $\nu_{sym}(ReF_{2c,c})$, $\nu_4(A_1)$, modes with the symmetric ReO_2 stretching mode $\nu_1(A_1)$ (Li^+, 332 cm^{-1} + 661 cm^{-1} = 993 cm^{-1}; Na^+, 326 cm^{-1} + 664 cm^{-1} = 990 cm^{-1}) giving rise to two groups of bands centered at 1008 (Li^+ and Na^+) and at 991 (Li^+) and 986 (Na^+) cm^{-1}. These lines are each factor-group split into an A_1 and a B_2 component. Fermi resonance is confirmed by the observation of only two bands at 972 and 1002 cm^{-1} for $[Cs][ReO_2F_4]$ in HF solution.

There is a strong dependency of the frequencies on the polarizing strength of the cation with the frequencies decreasing from Li^+ to $N(CH_3)_4^+$. A significant increase in frequencies is noted in going from $[Cs][ReO_2F_4]$ solid to $[Cs][ReO_2F_4]$ in HF solution and likely arises from hydrogen bonding interactions. The solvent dependence of the frequencies is consistent with the exchange behavior observed in the ^{19}F NMR spectrum for a solution of $[Cs][ReO_2F_4]$ in HF (see Characterization by NMR Spectroscopy).

$K^+Re_2O_4F_7^-$. Vibrational assignments for the $Re_2O_4F_7^-$ anion in $[K][Re_2O_4F_7]$ and in $[K][Re_2O_4F_7]\cdot 2ReO_2F_3$ were made under C_2 symmetry (structure III) for which a total of 33 vibrational modes are predicted (18A + 15B), all of which are Raman and infrared active. Assignments of the anion modes were also made by comparison with the isoelectronic $Os_2O_4F_7^+$ cation.[7] The spectrum of $[K][ReO_2F_7]$ could only be obtained for the single, randomly orientated crystal used in the X-ray structure determination.

The three Re−O stretches appear at significantly higher frequencies than in the $[K][ReO_2F_4]$ salt, which is consistent with a decrease in the polarity of the Re−O bonds resulting from the greater delocalization of the negative charge afforded by the larger $Re_2O_4F_7^-$ anion. The broad band at 554 cm^{-1} is tentatively assigned to $\nu_{as}(ReF_bRe')$, whereas the corresponding mode in $Os_2O_4F_7^+$ [7] was assigned to a very broad band at 492 (AsF_6^-) and 495 ($Sb_2F_{11}^-$) cm^{-1} and is presumed to be lower in the isoelectronic osmium cation because of the higher electronegativity of Os(VIII).

ReO_2F_3. Assignments for $(ReO_2F_3)_\infty$ and for $(ReO_2F_3)_\infty$ in $[K][Re_2O_4F_7]\cdot 2ReO_2F_3$ are primarily based on those for $(TcO_2F_3)_\infty$,[9] monomeric ReO_2F_3,[6] and $ReO_2F_4^-$ in which the environment around Re is very similar to that in $(ReO_2F_3)_\infty$. Moreover, the $F_{c,t}$ bond lengths in $ReO_2F_4^-$ are very similar to the Re−F_b bond lengths in the polymer. Coupling between different ReO_2F_4 units in the chains was initially assumed to be weak. For an uncoupled *cis*-ReO_2F_4 unit of C_{2v} point symmetry, all 15 vibrational modes having the symmetries $6A_1 + 2A_2 + 4B_1 + 3B_2$, with the [$O_t$, O_t, Re, F_b, F_b] plane taken as the $\sigma(xz)$ plane (structure IV), are expected to be Raman and

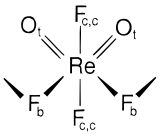

Structure IV

infrared active. Additional modes associated with Re−F_b−Re bridges are not accounted for in this analysis. Their expected low frequencies and intensities make their observation and assignment tentative.

The splittings observed for several bands in the spectrum of $(ReO_2F_3)_\infty$ in $[K][Re_2O_4F_7]\cdot 2ReO_2F_3$ are in agreement with the factor-group analysis which takes into account couplings between adjacent $(ReO_2F_3)_\infty$ chains in the crystal lattice. A further splitting is observed for the high-frequency band centered at 1021 cm^{-1} and likely arises from coupling of adjacent ReO_2F_4 units within the polymer chains. The majority of the bands are split in the spectrum of $(ReO_2F_3)_\infty$, for which, in the absence of a crystal structure, no factor-group analysis could be performed, but it is reasonable to assume that this splitting arises from coupling of ReO_2F_4 units of adjacent polymer chains in the unit cell.

The value observed for the ReO_2 scissoring mode, 412 cm^{-1}, is similar to the one in $ReO_2F_4^-$ ($N(CH_3)_4^+$: 401, 419 cm^{-1}) and is significantly different from that of monomeric ReO_2F_3.[6] The difference is likely related to the difference in the O−Re−O angles, with $\delta_{sciss}(ReO_2)$ occurring at lower frequency in the ReO_2F_3 monomer, where the O−Re−O angle is more open (110°) than in $(ReO_2F_3)_\infty$ (102°).

$[Cs][Re_3O_6F_{10}]$. Assignments are based on those for $Re_2O_4F_7^-$ and $(ReO_2F_3)_\infty$. The $Re_3O_6F_{10}^-$ anion contains a C_{2v} ReO_2F_4 unit bridging two ReO_2F_3 units, each having C_s symmetry and not related to each other by crystal symmetry (structure V). The

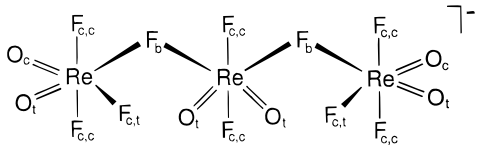

Structure V

symmetry of the anion is C_1, with a total of 53 A modes which are Raman and infrared active in the fully coupled system. In general, the frequencies are found to be higher than those of the corresponding modes in $ReO_2F_4^-$ and $Re_2O_4F_7^-$ and is attributed to the greater charge delocalization in the $Re_3O_6F_{10}^-$ anion. Moreover, the vibrational modes associated with the central rhenium atom occur at higher frequencies than those associated with the terminal rhenium atoms and are consistent with more localization of the anion charge on the terminal ReO_2F_3 groups (see Computational Results).

$ReO_2F_3(CH_3CN)$. The Raman spectrum was assigned on the basis of the energy-minimized structure determined by LDFT calculations (structure II), solution polarization measurements, and comparison with the Raman spectra of CH_3CN,[55] monomeric ReO_2F_3,[6] $ReO_2F_4^-$, and $TcO_2F_3(CH_3CN)$.[24] The adduct is expected to possess C_s symmetry for which 30 Raman and infrared active vibrational modes are predicted (19A′ + 11A″).

The bands occurring at 944−974 and 1001 cm^{-1} are similar to the asymmetric and symmetric ReO_2 stretching modes observed in related *cis*-dioxorhenium anions discussed in this paper. Their mode descriptions are complicated by coupling with the C−C and Re−N stretches as well as with CCN and CH_3 deformations. These bands appear at low frequency with respect to the corresponding bands in monomeric ReO_2F_3[6] and at high frequency with respect to that of $[N(CH_3)_4][ReO_2F_4]$, which is consistent with the lower base strength of CH_3CN with respect to that of F^- ion. However, LDFT calculations for $TcO_2F_3(CH_3CN)$[24] show that the antisymmetric $TcF_{2c,c}$ stretch is strongly coupled with the $TcF_{c,t}$ stretch. The ReO_2 bending mode is assigned to the strong band at 389 cm^{-1}, which is consistent with what is observed in the model compounds.

The vibrational modes of complexed CH_3CN above 1350 cm^{-1} and that at 944 cm^{-1} are readily assigned by comparison with those of free CH_3CN (Table 5, footnote *c*) and are similar to those observed for $TcO_2F_3(CH_3CN)$[24] and other metal complexes.[56] The bands assigned at ν_5(E), 3004; $\nu_1(A_1)$, 2945; $\nu_2(A_1)$, 2254; ν_6(E), 1447; $\nu_3(A_1)$, 1375; and $\nu_4(A_1)$, 918 cm^{-1}, in free CH_3CN are shifted to 3016, 2947, 2297/2323, 1412, 1367, and 944 cm^{-1}, respectively, in $ReO_2F_3(CH_3CN)$ and are generally in accord with frequency shifts observed in metal cation complexes, such as $M(CH_3CN)_6^{2+}$ (M = Sr, Ca, Mn, Fe, Co, Ni).[56]

Computational Results. Density functional theory has been shown to be a good method for predicting the geometries and vibrational spectra for transition metal compounds.[57] In our previous studies on osmium and technetium oxide fluorides,[20,24] we found that the local level yielded better structural and vibrational predictions than did calculations with gradient (nonlocal) corrections.

Molecular Geometries. The molecular geometries were initially optimized at the local density functional theory (LDFT)

(55) (a) Günthard, H. H.; Kováts, E. *Helv. Chim. Acta* **1952**, *145*, 1191. (b) Yamadera, R.; Kremm, S. *Spectrochim. Acta, Part A* **1968**, *24*, 1677.
(56) Reedijk, J.; Zuur, A. P.; Groeneveld, W. L. *Rec. Trav. Chim.* **1967**, *86*, 1127.
(57) Sosa, C.; Andzelm, J.; Elkin, B. C.; Wimmer, E.; Dobbs, K. D.; Dixon, D. A. *J. Phys. Chem.* **1992**, *96*, 6630.

level with a polarized double-ζ basis set (DZVP) (Table 2). Unless specified, the results discussed are at the LDFT level. In general, and as previously observed for related systems, the NLDFT values for the geometrical parameters are longer than the LDFT values.

The calculated geometric parameters for monomeric ReO_2F_3[8] (structure VI) have been reported previously along with those

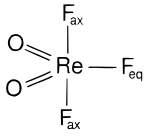

Structure VI

of the isoelectronic $OsO_2F_3^+$ cation. The structure was predicted to have C_{2v} point symmetry[58] with the two oxygen atoms and one fluorine atom (F_{eq}) in the equatorial plane of the trigonal bipyramid. These calculated values can now be compared with the observed values for $ReO_2F_4^-$ and those of $(ReO_2F_3)_\infty$. The Re−O bond distance in ReO_2F_3 is predicted to be 1.705 Å in contrast with the shorter experimental Re−O bond distances in $ReO_2F_4^-$ (1.678(8) Å) and $(ReO_2F_3)_\infty$ (1.676(8) Å). Unlike monomeric TcO_2F_3, where the Tc−F_{eq} and Tc−F_{ax} bond lengths were predicted to be the same,[24] the Re−F_{eq} bond (1.894 Å) in ReO_2F_3 is predicted to be longer than the Re−F_{ax} bonds (1.876 Å). The Re−F_{eq} bond is comparable to the Re−$F_{c,c}$ bonds in $ReO_2F_4^-$ (1.867(8) Å) and in $(ReO_2F_3)_\infty$ (1.834(7) and 1.854-(7) Å) while, as expected, the Re−F_{ax} bond is found to be shorter than the Re−$F_{c,t}$ and Re−F_b bond distances in $ReO_2F_4^-$ (2.002-(7) Å) and in $(ReO_2F_3)_\infty$ (2.102(6) Å). The O−Re−O and F_{ax}−Re−F_{ax} angles differ from the ideal 120 and 180° angles by 10 and 22°, respectively, showing that the O−Re−O angle is closing down and that the axial fluorines are bent away from the oxygens, toward the equatorial fluorine as in $ReO_2F_4^-$ and $(ReO_2F_3)_\infty$. The F_{eq}−Re−F_{ax}, O−Re−F_{ax}, and O−Re−F_{eq} angle values are the averages of their counterparts in the experimental structures of $ReO_2F_4^-$ and $(ReO_2F_3)_\infty$. Attempts to optimize the D_{3h} structure of monomeric ReO_2F_3 led to the C_{2v} structure. An approximately optimized D_{3h} structure with an Re−O bond length of 1.78 Å and an Re−F bond length of 1.85 Å is 54.5 kcal mol^{-1} above the C_{2v} structure at the LDFT level.

The lowest energy structure for $ReO_2F_4^-$ is the *cis*-dioxo structure (C_{2v} point symmetry) and is 32.2 kcal mol^{-1} more stable than the *trans*-dioxo structure (D_{4h} point symmetry) which has three imaginary frequencies. The calculated Re−O bond distance (1.913 Å) is 0.06 Å longer than that of $ReO_2F_4^-$ in the crystal structure. A similar difference has been found for the $TcO_2F_4^-$ anion, and the origin of the difference has been previously discussed.[24] The calculated Re−$F_{c,t}$ bond lengths (1.965 Å) are longer than the Re−$F_{c,c}$ bond lengths (1.913 Å) following the experimental trend, even though the calculated values for the Re−$F_{c,c}$ and Re−$F_{c,t}$ bond lengths are 0.046 Å longer and 0.037 Å shorter, respectively, than the experimental values. This suggests that there is a strong interaction between Li^+ and the $F_{c,t}$ atoms trans to the O atoms in the crystal. As expected for a structure to which a fluoride ion has been added, all Re−F bond distances are longer than those in monomeric ReO_2F_3. There is good agreement between the calculated and the observed angles, and as noted for $TcO_2F_4^-$, the largest differences occur for the angles involving the most ionic bonds, i.e., the fluorines trans to the oxygens, namely, $F_{c,t}$−Re−$F_{c,t}$ and $F_{c,t}$−Re−$F_{c,c}$.

(58) The nomenclature used for describing the equatorial fluorine (F_{eq}) and axial fluorine (F_{ax}) is identical to that used in ref 8.

As previously observed for the $TcO_2F_3(CH_3CN)$ adduct,[24] the energy-minimized structure for $ReO_2F_3(CH_3CN)$ is a *cis*-dioxo arrangement in which the CH_3CN molecule is coordinated trans to an oxygen. The geometrical parameters calculated for the $ReO_2F_3(CH_3CN)$ adduct are very similar to those observed for $(ReO_2F_3)_\infty$ with few changes. The bond distances for the Re−O bonds differ by 0.008 Å with the Re−O_t bond trans to the Re−N bond being shorter. The Re−$F_{c,t}$ bond trans to Re−O_c is significantly lengthened (1.949 Å) when compared to the other Re−$F_{c,c}$ bonds (1.872 and 1.880 Å). The CH_3CN moiety is essentially the same as that of free CH_3CN with C−C, 1.440 Å, and C−N, 1.164 Å. The long Re−N bond (2.316 Å) is consistent with a weaker donor−acceptor type interaction as compared to the more ionic interactions of O and F with Re. A similar trend was calculated for the Tc−N bond in $TcO_2F_3(CH_3CN)$.[24] The O_c−Re−O_t angle decreases by about 3° and one $F_{c,t}$−Re−O_c angle (154.3°) decreases by about 15° with the other $F_{c,t}$−Re−O_t angle (93.4°) increasing by a similar amount relative to $(ReO_2F_3)_\infty$. The $F_{c,c}$−Re−$F_{c,c}$ angle decreases by only 1°.

The calculated geometry for $Re_2O_4F_7^-$ shows some significant differences when compared to the experimental crystal structure. As expected, the calculated Re−O_t bond is longer than the experimental value by 0.05 Å. However, the calculated value for the Re−O_c bond is shorter than the experimental one by 0.03 Å suggesting that the K^+ counterion is strongly interacting with these oxygens. The calculated value for the Re−$F_{c,c}$ bond is characteristic of other Re(VII)−F bond lengths, on the order of 1.9 Å, and is ∼0.1 Å longer than the experimental Re(1)−F(3) value (1.783(8) Å; see X-ray Crystal Structures). Within the calculated Re−$F_{c,c}$ and Re−$F_{c,t}$ bonds, the expected trend, Re−$F_{c,c}$ < Re−$F_{c,t}$, is followed. The calculated value for the Re−F_b distance (2.125 Å) is in good agreement with the experimental value of 2.155 Å indicating that the bridging fluoride ion has a significant covalent interaction with both Re atoms. The calculated angles are in reasonable agreement with the experimental values except for the Re−F_b−Re angle where the calculated value is near linear (179.8°) whereas the experimental value is 143.3°. This discrepancy most likely arises from the fact that within the crystal the anions and cations are not isolated but, rather, there are significant electrostatic interactions between the cation and various O and F atoms of the anion. This could easily lead to a distortion of the bridge bond angle to maximize these interactions.

The calculated geometry for $Re_3O_6F_{10}^-$ is in very good agreement with the experimental crystal structure. As observed for all other related systems, the calculated Re−O and Re−F bond distances are slightly longer than the experimental values, except for Re(1)−F(4) and Re(3)−F(8). The largest discrepancies for the angles are observed for the two Re−F_b−Re angles which are found to be larger by 37° (Re(1)−F(4)−Re(2)) and smaller by 10° (Re(2)−F(7)−Re(3)), respectively. As noted for $Re_2O_4F_7^-$, these discrepancies most likely reflect the fact that the anion is not isolated in the crystal structure. This point is substantiated by the observation that the largest discrepancies occur for the Re(1)−F(4)−Re(2) bridge angle which is most affected by anion−cation contacts (see X-ray Crystal Structures).

Charges, Mayer Bond Valencies, and Mayer Bond Orders. A complete listing of the calculated charges, valencies, and bond orders is given in Table S10 (Supporting Information). The DZVP2 charges show the rhenium of the ReO_2F_3 monomer to have a charge of +1.94 e and negative charges of about −0.40 e on the oxygen and fluorine atoms. The Mayer valencies[59] show a valency of 5.95 for rhenium with valencies of 2.35 for oxygen

and 1.03 and 1.08 for the F_{eq} and F_{ax} atoms, respectively. The Mayer bond order is 1.81 for the Re−O bond showing that this bond is essentially a double bond whereas the Re−F bond orders, 0.77 and 0.79, indicate that these bonds have significant ionic characters.

For $ReO_2F_4^-$, the addition of a fluoride ion only slightly diminishes the charge on rhenium to +1.89 e. Most of the additional negative charge is equally distributed among the oxygen and fluorine atoms with charges ranging from −0.46 to −0.50 e. When compared to monomeric ReO_2F_3,[7] the Mayer valency at rhenium increases slightly to 6.09, at the DZVP2/PP level. A much larger increase was observed from TcO_2F_3 (6.27) to $TcO_2F_4^-$ (6.66).[24] The smaller change for the rhenium compound is consistent with the fact that Re is larger than Tc and hence would be less affected by the number of directly bonded ligands. The empirical bond valency of 7.09 derived using the method of Brown[33] (Table 2) is not in good agreement with the more rigorously derived and calculated Mayer value. The oxygen and fluorine valencies decrease somewhat in the anion to 2.27 (Re−O), 0.93 (Re−$F_{c,c}$), and 0.86 (Re−$F_{c,t}$). The Mayer bond orders also decrease in going from the ReO_2F_3 monomer[7] to the $ReO_2F_4^-$ anion with bond orders of 1.73 (Re−O) and 0.63 (Re−$F_{c,t}$) and 0.67 (Re−$F_{c,c}$).

The charges for the $ReO_2F_3(CH_3CN)$ adduct show some changes from that of monomeric ReO_2F_3 with the rhenium having less positive charge, +1.88 e as compared to +1.94 e in ReO_2F_3. The valency at rhenium increases from 5.95 in ReO_2F_3 to 6.03 in the adduct showing a weak interaction with the nitrogen atom that is consistent with the Mayer bond order of 0.23 for the Re−N bond. All of this behavior is similar to that found for the analogous Tc species.[24]

For $Re_2O_4F_7^-$ and $Re_3O_6F_{10}^-$ (values related to the trimer are given in parentheses), calculations show that $^2/_3$ of the charge is localized on the bridging fluorine atom(s). The rhenium atom charge is essentially unchanged (1.95 (1.94)) as compared to the charge on rhenium in ReO_2F_3 so that the remaining charge ($^1/_3$) is distributed over the four (six) oxygen atoms and the remaining six (nine) fluorine atoms. The Mayer valencies are very similar to those of monomeric ReO_2F_3 except that the terminal $F_{c,t}$ and $F_{c,c}$ atoms have slightly lower valencies. The F_b valency is only 0.50 (0.53), consistent with the long Re−F_b bonds and their high negative charge. The Mayer bond orders are consistent with the bond distances and valencies. We note that, in $Re_2O_4F_7^-$, the Re−F(2) bond order is lower than the rest (0.69) and is comparable to the lower Re−F bond order in $ReO_2F_4^-$ (0.63). The Re−F_b bond orders are small, 0.17 (0.12, 0.13), consistent with the long calculated and observed Re−F_b bond lengths.

The valence orbital populations on the Re atoms show that the electrons are predominantly in the d orbitals. For monomeric ReO_2F_3, there are 4.86 e in the valence d orbitals and 0.17 e in the valence p orbitals at the DZVP2/PP/LDFT level. For $ReO_2F_4^-$, there are only small changes in the populations on the rhenium atom, consistent with the atomic charges changing mostly on the oxygen and fluorine atoms. For $Re_2O_4F_7^-$ and $Re_3O_6F_{10}^-$, the d orbital populations average 4.87 e, showing essentially no change from those of monomeric ReO_2F_3.

NMR Chemical Shifts. It is now possible to calculate NMR chemical shifts by *ab initio* theoretical methods (Table 6). We have used the GIAO approach[60] for treating the gauge problem. The standards used for the relative chemical shift calculations are $CFCl_3$ for ^{19}F (σ = 142.0 ppm calculated) and H_2O for ^{17}O (σ = 322.1 ppm calculated). The ^{17}O chemical shifts of ReO_2F_3 monomer and $ReO_2F_4^-$ are predicted to be shifted to low frequency relative to the standard by −906 ppm for $ReO_2F_4^-$ and −882 ppm for the free ReO_2F_3. The ^{19}F chemical shifts also exhibit interesting behaviors. The fluorine resonances in $ReO_2F_4^-$ are predicted at −16.3 ppm for $F_{c,c}$ and 3.9 ppm for $F_{c,t}$ giving a chemical shift difference of 20.2 ppm as compared to the experimental difference of 10.4 ppm. Although the computed shifts for $ReO_2F_4^-$ are off in absolute magnitude by about 50 ppm, the chemical shift order is as expected; i.e., the fluorines trans to oxygens are shifted to higher frequency relative to the fluorines cis to oxygens. The ^{19}F chemical shifts for ReO_2F_3 are predicted to be more shielded for the F_{ax} (−93.1 ppm) as compared to $F_{c,c}$ of $ReO_2F_4^-$, whereas the F_{eq} chemical shift is predicted to occur at higher frequency (1.9 ppm), similar to the chemical shift of $F_{c,t}$ in the $ReO_2F_4^-$ anion. The same calculated and experimental ^{19}F chemical shift trends were found for $TcO_2F_4^-$ and TcO_2F_3.[24]

Table 6. ^{19}F NMR Shifts (ppm) for ReO_2F_3, $ReO_2F_4^-$, and $Re_2O_4F_7^-$

				σ		
	atom	diamag	paramag	absolute	relative	expt
ReO_2F_3	F_{ax}	469.7	−420.7	48.9	−93.1	
	F_{eq}	472.3	−474.2	−1.9	1.9	
	O	398.8	−958.6	−559.8	−881.9	
$ReO_2F_4^-$	$F_{c,c}$	471.1	−345.4	125.7	−16.3	−64.2[a]
	$F_{c,t}$	471.0	−325.1	145.9	3.9	−53.8[a]
	O	403.2	−987.4	−584.2	−906.3	
$Re_2O_4F_7^-$	$F_{c,t}$	473.1	−379.1	94.1	−47.9	−38.6[b]
	O_c	402.0	−985.7	−583.7	−905.8	
	O_t	396.7	−985.0	−588.3	−910.4	
	F_b	484.5	−125.9	358.6	216.6	−141.2[b]
	$F_{c,c}$	472.7	−385.0	87.8	−54.2	−28.8[b]
	$F_{c,c}$	472.9	−369.0	103.9	−38.1	−28.8[b]

[a] Recorded at 30 °C in CH_3CN solvent. [b] Recorded at −40 °C in CH_3CN solvent.

Vibrational Frequencies. In general, there is good agreement between the calculated and experimental frequency values for $ReO_2F_4^-$ even though there is a strong dependence upon the nature of the cation in the experimental spectra (Table 3). The best agreement is observed at the LDFT level and with the $[N(CH_3)_4][ReO_2F_4]$ salt where no or very weak anion cation contacts are expected. Similar results have been obtained for $TcO_2F_4^-$.[24] The LDFT and NLDFT values are identical for the modes involving Re−O stretches and ReO_2 bend, but they are smaller than the experimental values. This difficulty in predicting the modes involving O atoms was also found in calculations on technetium[24] and osmium oxide fluorides[7,20b] and on monomeric ReO_2F_3[7] and is consistent with there being too little repulsion between the nonbonded O atoms. At the LDFT level, the two highest calculated Re−F stretches are lower than the experimental values whereas the two lowest Re−F stretches are predicted to be higher than the experimental values.

Calculations confirm that the vibrational modes of the fluorine-bridged ReO_2F_3 groups of $Re_2O_4F_7^-$ are weakly coupled. The Re−O stretches are shifted to higher frequency than in the $ReO_2F_4^-$ anion, and the splitting in the two types of Re−O stretches has slightly increased. As for all other related compounds, the ReO stretches and ReO_2 bends are found to be

(59) (a) Mayer, I. *Chem. Phys. Lett.* **1983**, *97*, 270. (b) Mayer, I. *Theor. Chim. Acta* **1985**, *67*, 315. (c) Mayer, I. *J. Quantum Chem.* **1986**, *29*, 73. (d) Mayer, I. *J. Quantum Chem.* **1986**, *29*, 477.

(60) (a) Cheeseman, J. R.; Trucks, G. W.; Keith, T. A.; Frisch, M. J. *J. Chem. Phys.* **1996**, *104*, 5497. (b) London, F. *J. Phys. Radium (Paris)* **1937**, *8*, 397. (c) Ditchfield, R. *Mol. Phys.* **1974**, *27*, 789. (d) Wolinski, K.; Hinton, J. F.; Pulay, P. *J. Am. Chem. Soc.* **1990**, *112*, 8251.

lower than the experimental values. The Re−F stretches show two groups of bands, one near 650 cm^{-1} and one near 580 cm^{-1}. The antisymmetric bridging stretch is predicted to be at 512 cm^{-1} with the symmetric stretch much lower at only 108 cm^{-1}. The high frequency of the antisymmetric Re−F_b−Re stretch shows that the anion does not dissociate readily, but the low frequency of the symmetric stretch shows that the two ReO_2F_3 groups are not strongly coupled. The ReO_2 bends are shifted to higher frequency in $Re_2O_4F_7^-$ as compared to $ReO_2F_4^-$, consistent with the change in the ReO stretching frequencies. Most of the low-frequency modes involve rigid motions of the ReO_2F_3 groups.

The calculated vibrational frequencies of the $ReO_2F_3(CH_3CN)$ adduct also show good agreement with the experimental values (Table 5). As obtained for $TcO_2F_3(CH_3CN)$,[24] the modes associated with the CH_3 group agree and the CN triple bond stretch which is predicted to be at 2373 cm^{-1} compared to the experimental value of 2297 cm^{-1}. The Re−O modes split apart with the Re−O_t mode occurring at higher frequency than the Re−O_c mode. The Re−N stretch occurs at a much lower frequency, i.e., 221 and 212 cm^{-1}, although it also mixes with the Re−O_c stretch at 976 cm^{-1}. The remaining bands of the spectrum show good agreement with the ReO_2 bends, again predicted higher than the experimental values.

Fluoride Ion Affinities. The fluoride ion affinity (FA) is defined by analogy with a proton affinity as the negative of the enthalpy change of reaction 9. If the fluoride ion affinity is

$$A + F^- \rightarrow AF^- \quad (9)$$

positive, then this is an exothermic process and A can bind F^-. Because of the difficulty in calculating the electron affinity of fluorine, the relative fluoride ion affinities were calculated as shown in reaction 10. If FA(A) is known, then FA(B) can be

$$AF^- + B \rightarrow A + BF^- \quad (10)$$

calculated. The fluoride ion affinity of COF_2, FA(COF_2), was chosen as a standard, and it was previously shown that FA(COF_2) is 49.9 kcal mol^{-1} on the basis of the revised value of FA(HF).[61] Thus, the calculated FA(ReO_2F_3) was found to be 78.0 kcal mol^{-1} at the DZVP2/PP/LDFT level and 79.3 kcal mol^{-1} at the DZVP/PP/NLDFT level. These values are slightly larger than FA(TcO_2F_3), which are 74.2 kcal mol^{-1} at the LDFT level and 75.7 kcal mol^{-1} at the NLDFT level and are consistent with the higher Lewis acidity of ReO_2F_3 noted in this work toward CH_3CN and F^- ion.

Conclusions

A new high-yield, high-purity synthesis of ReO_2F_3 was developed and involves the fluorination of Re_2O_7 in anhydrous HF using XeF_6. The structure of ReO_2F_3 consists of infinite chains of fluorine-bridged ReO_2F_4 units and is analogous to that of TcO_2F_3. The Lewis-acid properties of ReO_2F_3 toward fluoride ion and CH_3CN were investigated and resulted in the syntheses of several $[M][ReO_2F_4]$ salts (M = Li, Na, K, Cs, $N(CH_3)_4$) and the $ReO_2F_3(CH_3CN)$ adduct. Comparison of the Raman and ^{19}F NMR spectroscopic data indicate that ReO_2F_3 is a stronger Lewis acid than TcO_2F_3,[24] and this is confirmed by their calculated relative fluoride ion affinities. The $ReO_2F_4^-$ anion reacts with ReO_2F_3 to form the fluorine-bridged $Re_2O_4F_7^-$ and $Re_3O_6F_{10}^-$ anions. The $Re_3O_6F_{10}^-$ anion only forms when more acidic solvents and cations are used. All three anions, $ReO_2F_3(CH_3CN)$, and ReO_2F_3 adopt the *cis*-dioxo arrangement which is a feature in common with all other dioxo species of d^0 transition metals. The trans influence of the oxo ligands is significant in these compounds and results in a lengthening of the Re−F bonds trans to the oxygens as well as enhancement of their lability. The energy-minimized geometries determined from density functional theory calculations are in agreement with the structures determined by X-ray crystallography and by NMR and Raman spectroscopy.

Experimental Section

Apparatus and Materials. Preparative apparatus and procedures have been described previously.[24] Single crystals were selected and mounted in glass Lindemann capillaries inside a drybox and then heat sealed. Crystals were stored at −10 °C, unless otherwise indicated, prior to mounting on the diffractometer.

Starting materials which were dried, purified, prepared by standard literature methods, or used without further purification, were the following: $[N(CH_3)_4][F]$,[62] F_2 (Air Products), H_2 (99.99%, Canadian Liquid Air), O_2 (Canadian Liquid Air, Zero Grade, 99.99%), XeF_6[63] (ascertained to be free of XeF_4 contaminant using Raman spectroscopy), CsF (Merck, 99+%),[64] and rhenium powder (Cleveland Refractory Metals, 325 mesh). The solvents, CH_3CN (HPLC Grade, Caledon Laboratories Ltd.)[65] and HF (Harshaw Chemical Co.)[66] were dried/purified by the standard literature methods.

Re_2O_7. The synthesis of Re_2O_7 was carried out by heating rhenium powder (4.945 g, 2.655 mmol) that had been previously heated to red heat under H_2 and dried under vacuum in an excess of dry O_2 inside a closed quartz reaction tube. The procedure was analogous to that used to prepare Tc_2O_7.[9] The yield was 5.900 g, 1.218 mmol (91.7%), and the product was a yellow to yellow green crystalline material.

ReO_2F_3. In the drybox, 1.0293 g (2.1249 mmol) of Re_2O_7 was weighed into a T-reactor. The reactor was transferred to a metal vacuum line, and anhydrous HF (6 mL) was condensed into the reactor at −196 °C. A known amount of XeF_6 (0.8149 g, 3.323 mmol) was condensed from an FEP weighing vessel into the reactor at −196 °C. Upon warming of the reactor and its contents to room temperature, a white precipitate of ReO_2F_3 formed immediately. The insoluble product was separated from the soluble byproducts (see reactions 1−3), by decanting the supernatant into the sidearm of the reactor. The solvent was pumped off on the metal vacuum line while the ReO_2F_3 was cooled to 0 °C to prevent its slow sublimation and was recovered as a friable white solid in the drybox (1.1106 g, 4.0357 mmol, 95.0% yield), melting point 113−116 °C. ***Caution:*** *The $XeOF_4$-containing decantate was disposed of by slowly pouring the cold HF solution (−78 °C) into a mixture of ice and NaOH solution inside a fume hood.*

$ReO_2F_3(CH_3CN)$. In the drybox, ReO_2F_3 (0.2114 g, 0.7682 mmol) was weighed into a $^1/_4$-in. o.d. FEP reaction vessel fitted with a Kel-F valve. Dry CH_3CN (ca. 1 mL) was condensed onto the solid which dissolved completely at room temperature to yield a pale yellow solution. The excess CH_3CN was pumped off at 0 °C for 12 h, and a white powder was isolated which was stable at room temperature. A sample for NMR spectroscopy was prepared by dissolving 0.0402 g (0.146 mmol) of ReO_2F_3 in 0.0100 g (0.244 mmol) of dry CH_3CN in a 4-mm FEP tube followed by addition of ca. 0.3 mL of SO_2ClF.

$[M][ReO_2F_4]$ (M = Li, Na, Cs) and Crystal Growth of $[Li][ReO_2F_4]$. In the drybox, ReO_2F_3, 0.3868 g (1.406 mmol), and LiF, 0.0369 g (1.42 mmol), were loaded into one arm of a $^1/_4$-in. o.d. FEP T-reactor, and a Kel-F valve was attached. Anhydrous HF (ca. 1 mL) was condensed onto the reactants under static vacuum at −196 °C. At room temperature, a pale, yellow solid in a yellow solution was observed. The yellow solid completely dissolved on addition of more HF. Enough HF was then removed to precipitate ca. 50 mg of solid

(61) Krespan, C. G.; Dixon, D. A. *J. Fluorine Chem.* **1966**, *11*, 117.
(62) Christe, K. O.; Wilson, W. W.; Wilson, R. D.; Bau, R.; Feng, J. A. *J. Am. Chem. Soc.* **1990**, *112*, 7619.
(63) Chernick, C. L.; Malm, J. G. *Inorg. Synth.* **1966**, *8*, 258.
(64) Christe, K. O.; Curtis, E. C.; Dixon, D. A.; Mercier, H. P. A.; Sanders, J. C. P.; Schrobilgen, G. J. *J. Am. Chem. Soc.* **1991**, *113*, 3351.
(65) Christe, K. O.; Wilson, W. W. *J. Fluorine Chem.* **1990**, *47*, 117.
(66) Emara, A. A. A.; Schrobilgen, G. J. *Inorg. Chem.* **1992**, *31*, 1323.

$[Li][ReO_2F_4]$ at 20 °C. Both arms of the T-reactor were heated in water baths to 40 °C, and the yellow solution was decanted from the remaining solid into the free arm of the reactor. Both arms of the reactor were allowed to cool to 20 °C over an 8 h period, at the end of which yellow platelike crystals were obtained in the yellow solution. The supernatant solution was decanted back into the original reaction arm, and the solvent was removed under dynamic vacuum at 20 °C. The crystals showed no signs of decomposition under vacuum, nor did the yellow microcrystalline $[Li][ReO_2F_4]$ isolated in the other arm of the reaction vessel. After being sealed in Lindemann capillaries, the crystals were stored at room temperature since they were observed to powder below 0 °C. Analogous procedures were used to prepare $[Na][ReO_2F_4]$ [ReO_2F_3, 0.1597 g (0.5803 mmol), and NaF, 0.0291 g (0.693 mmol)] and $[Cs][ReO_2F_4]$ [ReO_2F_3, 0.1422 g (0.5167 mmol), and CsF, 0.0813 g (0.538 mmol)]. Removal of HF at room temperature provided quantitative yields of yellow, microcrystalline $[Na][ReO_2F_4]$ and $[Cs][ReO_2F_4]$. X-ray powder photographs confirmed that the Na^+ salt was isomorphous with $[Li][ReO_2F_4]$. The data indexed for a tetragonal cell, $a = 5.025(1)$ Å, $c = 9.207(1)$ Å, and $V = 232.5$ Å^3.

$[N(CH_3)_4][ReO_2F_4]$. In the drybox, ReO_2F_3 (0.4053 g, 1.473 mmol) was weighed into a $^1/_4$-in. o.d. FEP reactor. A stoichiometric amount of preweighed $[N(CH_3)_4][F]$ (0.1356 g, 1.456 mmol) was added to the reactor. Anhydrous HF (4 mL) was condensed into the reactor on a metal vacuum line at −196 °C. On being warmed to room temperature, the solids dissolved to give a pale yellow solution. Further addition of HF to the solution did not result in precipitation of ReO_2F_3. Removal of the solvent under dynamic vacuum resulted in 0.5236 g (1.421 mmol, 97.6% yield) of yellow microcrystalline $[N(CH_3)_4][ReO_2F_4]$.

$[N(CH_3)_4][Re_2O_4F_7]$. In the drybox, $[N(CH_3)_4][ReO_2F_4]$ (0.0457 g, 0.124 mmol) and ReO_2F_3 (0.0347 g, 0.126 mmol) were loaded into a $^1/_4$-in o.d. FEP tube fitted with a Kel-F valve. Approximately 0.5 mL of dry CH_3CN was condensed onto the solids, which dissolved completely at room temperature to yield a pale yellow solution. The reactor was then heat-sealed and stored at −196 °C until the NMR experiment was performed.

$[K][Re_2O_4F_7]$ and Crystal Growth of $[K][Re_2O_4F_7]$ and $[K][Re_2O_4F_7]\cdot 2ReO_2F_3$. $[K][Re_2O_4F_7]$. In the drybox, ReO_2F_3 (0.1514 g, 0.5502 mmol) and KF (0.0160 g, 0.2767 mmol) were loaded into a $^1/_4$-in o.d. FEP T-reactor fitted with a Kel-F valve. Anhydrous HF (ca. 0.5 mL) was condensed onto the solids, which partially dissolved at room temperature, forming a pale yellow solution and a white residue. The reactor was pressurized to 2 atm with dry nitrogen, and both arms of the reactor were warmed to 40 °C and agitated before decanting the supernatant into the empty arm of the reactor. Colorless plates grew over a 24 h period as the solution was allowed to cool to room temperature. The solution was decanted off the crystals, and the solvent was removed under dynamic vacuum and pumped for a further 24 h before transferring the reactor into a drybox.

$[K][Re_2O_4F_7]\cdot 2ReO_2F_3$. In the drybox, ReO_2F_3 (0.1573 g, 0.572 mmol) and KF (0.0173 g, 0.298 mmol) were loaded into a bent $^1/_4$-in o.d. FEP reactor fitted with a Kel-F valve. Anhydrous HF (ca. 0.3 mL) was distilled onto the solids, which partly dissolved at room temperature, forming a pale yellow solution and a white residue. The reactor was pressurized with dry nitrogen (1100 Torr), warmed to 40 °C, and sonicated for 5 min. The solution was then carefully decanted into the elbow of the reactor and submerged in a water bath at 45 °C and allowed to slowly cool to room temperature. Large colorless, crystalline plates and small needles formed after 48 h. The solution was decanted to the bottom of the reactor and pumped off, and the crystals were dried under dynamic vacuum for 24 h. Only the needles were found to diffract.

$[Cs][Re_3O_6F_{10}]$ and Crystal Growth. In the drybox, ReO_2F_3 (0.2039 g, 0.7409 mmol) and CsF (0.0439 g, 0.289 mmol) were weighed into one arm of a T-reactor fitted with $^3/_8$-in. o.d. FEP tubes and a Kel-F valve. Anhydrous HF (4 mL) was condensed onto the solids, and the reactor was pressurized to 2 atm with dry N_2. The tube containing anhydrous HF was heated to 40 °C and agitated. Over half (by volume) of the solid observed at room temperature dissolved at this point. The colorless supernatant solution was decanted into the free arm of the reactor, which had also been heated to 40 °C using a Dewar flask filled with warm water, and allowed to cool slowly to room temperature. Colorless needles and plates grew over a period of ∼8 h. Following X-ray data collection, the Raman spectrum of the single crystal was obtained.

Crystal Growth of $ReO_3F(CH_3CN)_2\cdot CH_3CN$. Crystals of $ReO_3F(CH_3CN)_2\cdot CH_3CN$ were grown from an NMR sample of ReO_2F_3 in CH_3CN by slow hydrolysis apparently resulting from diffusion of water through the thin wall of the FEP tube over a period of several months. The crystalline material that had initially formed was heated to 40 °C in a water bath to give a clear pale yellow solution and allowed to cool to room temperature over a period of 2 days, producing large cubic crystals. The FEP tube was transferred to a glovebag filled with dry nitrogen and cut open. The supernatant solvent was removed using a dry pipet, the tube containing the crystals was inserted into a larger FEP tube which was fitted with a Kel-F valve, and the remaining solvent was removed under dynamic vacuum for ca. 10 s.

Nuclear Magnetic Resonance Spectroscopy. NMR instrumentation and chemical shift referencing are described in ref 24. The ^{19}F NMR spectrum of $[N(CH_3)_4][ReO_2F_4]$ was acquired at 470.599 MHz in a 16 K memory with a spectral setting of 12 kHz, yielding an acquisition time of 0.668 s and data point resolution of 1.45 Hz/data point. The number of transients accumulated was 532; a pulse width of 1.0 μs and a line broadening of 1.0 Hz were used. The ^{19}F NMR spectrum of $[N(CH_3)_4][Re_2O_4F_7]$ was acquired at 282.409 MHz using a pulse width of 11 μs. A total of 500 transients were acquired in a 32K memory using a spectral width setting of 25 kHz, an acquisition time of 0.655 s, and a resolution of 1.53 Hz/data point. The ^{19}F NMR spectrum of $ReO_2F_3(CH_3CN)$ was acquired at 282.409 MHz using a pulse width of 3 μs. A total of 1655 transients were acquired in a 16K memory using a spectral width setting of 10 kHz, an acquisition time of 0.819 s, and a resolution of 1.22 Hz/data point. The ^1H NMR spectrum of $ReO_2F_3(CH_3CN)$ was acquired at 300.134 MHz using a pulse width of 2 μs. A total of 60 transients were acquired in a 16K memory using a spectral width setting of 3600 Hz, an acquisition time of 2.277 s, and a resolution of 0.44 Hz/data point. The ^{13}C NMR spectrum of $ReO_2F_3(CH_3CN)$ was acquired at 75.469 MHz using a pulse width of 2 μs. A total of 13 000 transients were acquired in a 16K memory using a spectral width setting of 25 kHz, an acquisition time of 0.328 s, and a resolution of 3.05 Hz/data point.

X-ray Structure Determinations of $[Li][ReO_2F_4]$, $[K][Re_2O_4F_7]$, $[K][Re_2O_4F_7]\cdot 2ReO_2F_3$, $[Cs][Re_3O_6F_{10}]$, and $ReO_3F(CH_3CN)_2\cdot CH_3CN$. Collection and Reduction of X-ray Data. The crystals of $[Li][ReO_2F_4]$, $[K][Re_2O_4F_7]$, and $[Cs][Re_3O_6F_{10}]$ were centered on a Siemens/Syntex $P2_1$ diffractometer, using silver radiation monochromatized with a graphite crystal ($\lambda = 0.560\,86$ Å). The collection and reduction of the X-ray data as well as the refinement of the structures were carried out in a similar manner for the three data sets. The experimental values for $[K][Re_2O_4F_7]$ and $[Cs][Re_3O_6F_{10}]$, when differing from those of $[Li][ReO_2F_4]$, are given in parentheses and brackets, respectively. Accurate cell dimensions were determined at $T = 24$ [−118] °C from a least-squares refinement of the setting angles (χ, ϕ, and 2θ) obtained from 21 (25) [27] accurately centered reflections (with 15.67 (15.42) [14.53]° ≤ 2θ ≤ 28.60 (29.79) [24.93]°) chosen from a variety of points in reciprocal space. Integrated diffraction intensities were collected using a $\theta-2\theta$ scan technique with scan rates varying from 1.5 to 14.65°/min (in 2θ) and a scan range of ±0.75 (0.5) [0.5]°. The data were collected with $0 \le h \le 9$ (6) [12], -9 (−6) [−17] ≤ $k \le 0$ (6) [17], and −16 (−18) [−18] ≤ $l \le 16$ (17) [18] and $3 \le 2\theta \le 60$ (40) [55]°. During data collection, the intensities of three standard reflections were monitored every 97 reflections. Over the course of data collection no decay was observed. A total of 2875 (1671) [6490] reflections were collected. A total of 666 (801) [6095] unique reflections remained after averaging of equivalent reflections of which 665 (801) [6026] were used for structure solution. Corrections were made for Lorentz and polarization effects, while absorption corrections were applied using the program DIFABS.[67]

Data for $[K][Re_2O_4F_7]\cdot 2ReO_2F_3$ and $ReO_3F(CH_3CN)_2\cdot CH_3CN$ were collected using a P4 Siemens diffractometer, equipped with a Siemens SMART 1K charge-coupled device (CCD) area detector (using the program SMART)[68] and a rotating anode using graphite-monochro-

(67) Walker, N.; Stuart, D. *Acta Crystallogr.* **1983**, *A39*, 158.

mated Mo Kα radiation ($\lambda = 0.710\,73$ Å). The crystal-to-detector distance was 3.991 cm, and the data collection was carried out in a 512×512 pixel mode using 2×2 pixel binning. A complete sphere of data was collected, to better than 0.8 Å resolution. Processing was carried out by using the program SAINT,[68] which applied Lorentz and polarization corrections to three-dimensionally integrated diffraction spots. The program SADABS[69] was used for the scaling of diffraction data, the application of a decay correction, and an empirical absorption correction based on redundant reflections.

Solution and Refinement of the Structures. Calculations were performed as previously described.[24] The program XPREP[70] was used to confirm the unit cell dimensions and the crystal lattice. A solution was obtained using Patterson ($[Li][ReO_2F_4]$, $[K][Re_2O_4F_7]$ and $[K][Re_2O_4F_7]\cdot 2ReO_2F_3$) and direct ($[Cs][Re_3O_6F_{10}]$) methods which located the Re atoms. The positions of all the fluorine, oxygen, and alkali metal (lithium, potassium, and cesium) atoms were revealed in successive difference Fourier syntheses. The oxygen and fluorine atoms were assigned on the basis of their bond lengths with rhenium. In view of the rather long Re(1)−O(2) and short Re(1)−F(3) bond lengths observed in both $[K][Re_2O_4F_7]$ and $[K][Re_2O_4F_7]\cdot 2ReO_2F_3$, a model involving a positional disorder between O(2) and F(3) was tentatively used to solve the structure but did not produce a satisfactory result. The final refinements were obtained by using data that had been corrected for absorption and by introducing anisotropic thermal parameters for all the atoms except for the Li atom which was kept isotropic. An extinction parameter was used for $[K][Re_2O_4F_7]\cdot 2ReO_2F_3$. During the final stages of the refinement, all reflections with $F^2 < -2\sigma(F^2)$ were suppressed and weighting factors recommended by the refinement program were introduced. In the final difference Fourier map, the maximum and minimum electron densities were located around the Re atoms.

No reasonable solution could be obtained for $ReO_3F(CH_3CN)_2\cdot CH_3CN$ in any of the tetragonal space groups proposed by the program XPREP.[70] The structure was, however, solved in $P\bar{1}$ and then in $P2_1/m$. It was then apparent that the crystal was twinned as a result of similar *a*- and *c*-axes and that the system was, in fact, orthorhombic. The twinning was modeled, and a solution was obtained in *Pnma* using a Patterson function which located the position of the rhenium atom. Successive difference Fourier syntheses revealed the positions of the light atoms. The hydrogen atoms were refined using a riding model. A positionally disordered solvent molecule was finally located, and the site occupancy factors (sof) were adjusted accordingly. In view of the symmetry of the molecule, a possible fluorine/oxygen positional disorder was considered. This possibility was dismissed because the Re−F bond length has a value characteristic of Re(VII)−F bonds found in other Re(VII) oxide fluoride species. Moreover, a positional disorder between F and O implied that the Re atom laid in the [O(1), O(1A), N(1), N(1A)] plane, which was not observed experimentally (see X-ray Crystal Structures). The final refinement was obtained by introducing anisotropic parameters for all the atoms except the hydrogen atoms, an extinction parameter, and the recommended weight factor.

Raman Spectroscopy. Raman spectra were recorded as previously described.[24] Holographic gratings were used for the prefilter (600 grooves mm^{-1}, blazed at 500 nm) and monochromator (1800 grooves mm^{-1}, blazed at 550 nm) stages. An Olympus metallurgical microscope (model BHSM-L-2) was used for focusing the excitation laser to a 1-μm spot on solid samples. Spectra were recorded at room temperature on powdered microcrystalline samples sealed in Pyrex melting point capillaries as well as on a single crystal of $[K][Re_2O_4F_7]$ sealed in a dry Lindemann capillary. The spectra were recorded at laser powers of 50−300 mW and slit settings corresponding to a resolution of 1 cm^{-1}. A total of 15 reads each having 45 s integration times were summed using a CCD detector. The spectra of $[Cs][ReO_2F_4]$ in HF were obtained directly in the FEP reaction vessel and were collected in the Raman macrochamber using a laser power of 600 mW. A total of 10 reads each having a 60 s integration time were summed. Polarization/depolarization measurements were made on this sample, but no quantitative ${}^{\parallel}I_n/{}^{\perp}I_n$ ratio was determined, because the measured radiation had been partially randomized by the FEP tube.

Computational Methods. Calculations were done as described previously.[24] The basis sets[71] for the carbon, oxygen, and fluorine atoms are of the form (721/51/1) (DZVP2) with a (7/3/3) fitting set. For hydrogen, the basis set has the form (4/1/1) and a fitting basis set of the form (4). For Re, a basis set in which the Re core electrons are treated with a pseudopotential[72] (PP) and the remaining electrons are treated with a polarized valence double-ζ basis set (43/4/32) was used with a fitting basis set of the form (5/5/5). This basis set is denoted DZVP2/PP.

Additional NMR calculations on ReO_2F_3 and $ReO_2F_4^-$ using the GIAO approach for treating the origin problem[60] were done with the program Gaussian94 on SGI computers.[73] These calculations were done at the local level with a large basis set denoted as TZ2PF on the oxygen and fluorine, and an effective core potential was used for Re. The basis set for the NMR calculations is of triple-ζ quality[74] for oxygen and fluorine augmented by two sets of d polarization functions each formed from two Gaussian functions and an f polarization function. The rhenium basis set is from ref 75 and has the form (5s5p4d) with an effective core potential with the 5s, 5p, 5d, and 6s in the valence space.

Acknowledgment. We thank the Natural Sciences and Engineering Research Council of Canada for support in the form of a research grant and for the award of a graduate scholarship to N.L., the donors of the Petroleum Research Fund, administered by the American Chemical Society, for support of this work under ACS-PRF No. 31198-AC3, and the National Science Foundation (U.S.A.) for the award of a NATO Postdoctoral Fellowship to W.J.C. The density functional theory calculations were performed under the auspices of the Office of Basic Energy Sciences, U.S. Department of Energy, under Contract DE-AC06-76RLO 1830 with the Battelle Memorial Institute, which operates the Pacific Northwest National Laboratory, a multiprogram national laboratory operated for the Department of Energy.

Supporting Information Available: Unit cell diagrams for $K^+Re_2O_4F_7^-$ and $K^+Re_2O_4F_7^-\cdot 2ReO_2F_3$, tables of X-ray data and charges, and X-ray crystallographic files, in CIF format, for the structure determinations of $[Li][ReO_2F_4]$, $[K][Re_2O_4F_7]$, $[K][Re_2O_4F_7]\cdot 2ReO_2F_3$, $[Cs][Re_3O_6F_{10}]$, and $ReO_3F(CH_3CN)_2\cdot CH_3CN$. This material is available free of charge via the Internet at http://pubs.acs.org.

IC980695T

(68) *SMART* and *SAINT*, release 4.05; Siemens Energy and Automation Inc.: Madison, WI, 1996.
(69) Sheldrick, G. M. SADABS (Siemens Area Detector Absorption Corrections), personal communication, 1996.
(70) Sheldrick, G. M. *SHELXTL*, release 5.03; Siemens Analytical X-ray Instruments Inc.: Madison, WI, 1994.
(71) Godbout, N.; Salahub, D. R.; Andzelm, J.; Wimmer, E. *Can. J. Chem.* **1992**, *70*, 560.
(72) (a) Chen, H.; Kraskowski, M.; Fitzgerald, G. *J. Chem. Phys.* **1993**, *98*, 8710. (b) Troullier, N.; Martins, J. L. *Phys. Rev. B* **1991**, *43*, 1993.
(73) Frisch, M. J.; Trucks, G. W.; Schlegel, H. B.; Gill, P. M. W.; Johnson, B. G.; Robb, M. A.; Cheeseman, J. R.; Keith, T. A.; Peterson, G. A.; Montgomery, J. A.; Raghavachari, K.; Al-Laham, M. A.; Zakrzewski, V. G.; Ortiz, J. V.; Foresman, J. B.; Cioslowski, J.; Stefanov, B. B.; Nanayakkara, A.; Challacombe, M.; Peng, C. Y.; Ayala, P. Y.; Chen, W.; Wong, M. W.; Andres, J. L.; Replogle, E. S.; Gomperts, R.; Martin, R. L.; Fox, D. J.; Binkley, J. S.; Defrees, D. J.; Baker, J.; Stewart, J. J. P.; Head-Gordon, M.; Gonzalez, C.; Pople, J. A. *Gaussian 94*; Gaussian, Inc.: Pittsburgh, PA, 1995.
(74) Dunning, T., Jr. *J. Chem. Phys.* **1971**, *55*, 716.
(75) (a) Reed, A. E.; Curtis, L. A.; Weinhold, F. *Chem. Rev.* **1988**, *88*, 899. (b) Foster, J. P.; Weinhold, F. J. *J. Am. Chem. Soc.* **1980**, *102*, 7211. (c) Reed, A. E.; Weinhold, F. *J. Chem. Phys.* **1983**, *78*, 4066. (d) Reed, A. E.; Weinstock, R. B.; Weinhold, F. *J. Chem. Phys.* **1985**, *83*, 735. (e) Reed, A. E.; Weinhold, F. *J. Chem. Phys.* **1985**, *83*, 1736.